Title

Central carbon metabolism switching in lytic versus temperate coral reef viral communities

Authors

Jacob Kelman[1,2*], Meena Khan[1,2*], Chibundu Umunna[1,2*], Russell Brainard[3], Grace Donohue[1,2], Rob Edwards[4], Natalie A Falta[1,2], Emma George[5,6], Eleanor Gorham[1,2], Juris Grasis[7], Kevin Green[5], Andreas Haas[5,8], Kimberly Halsey[9], Eric Hester[5,10], Summer Jacob[1], Aydin Loid Karatas[1,2,11], Yan Wei Lim[5], Mark Little[5,12], Stuart Sandin[13], Jessie Segnitz[1], Maya Serota[1], Natalia Shahwan[1], Giselle Simmons[1], Jennifer E Smith[13], Isha Tripathi[1,2], Linda Wegley Kelly[13], Lauren Woodward[1], Nickie Yang[1,2], Charles Young[14], Brian Zgliczynski[13], Forest Rohwer[5], Ben Knowles[1,2,15,16†]

* These authors contributed equally to this work.

Affiliations

[1] Department of Ecology and Evolutionary Biology, University of California, Los Angeles, California 90095, USA

[2] Institute for Quantitative and Computational Biosciences, University of California, Los Angeles, California 90095, USA

[3] R Ocean LLC, Kāne'ohe, Hawaii 96744, USA

[4] Flinders Accelerator for Microbiome Exploration, Flinders University, Bedford Park, South Australia 5042, Australia

[5] Biology Department, San Diego State University, San Diego, California 92182, USA

[6] Integrative Oceanography Division, Scripps Institution of Oceanography, University of California, San Diego, La Jolla, California 92093, USA

[7] School of Natural Sciences, University of California, Merced, Merced, California 95343, USA

[8] Department of Marine Microbiology and Biogeochemistry, NIOZ Royal Netherlands Institute for Sea Research, 1797 SZ 't Horntje (Texel), Netherlands

[9] Department of Microbiology, Oregon State University, Corvallis, Oregon 97331, USA

[10] NIZO Food Research B.V., Kernhemseweg 2, 6718 ZB Ede, Netherlands

[11] Department of Quantitative and Computational Biology, University of Southern California, Los Angeles, California, USA

[12] Department of Organismic and Evolutionary Biology, Harvard University, Cambridge, Massachusetts 02138, USA

[13] Marine Biology Research Division, Scripps Institution of Oceanography, University of California, San Diego, La Jolla, California 92093, USA
[14] Pacific Islands Ocean Observing System, University of Hawaii at Manoa, Honolulu, Hawaii 96822, USA
[15] California NanoSystems Institute, University of California, Los Angeles, California 90095, USA
[16] Institute of the Environment and Sustainability, University of California, Los Angeles, California 90095, USA

Correspondence
[†] Ben Knowles: bwknowles@ucla.edu

Main text length (Introduction, Methods, Results, and Discussion): 4743 words

List of Tables and Figures

Table 1: Central carbon metabolism genes shown in Figures 2, 3, and 4.

Figure 1: Correlations between metabolic function and community temperateness across the breadth of cellular metabolism (SEED Level 1).

Figure 2: Correlation between central carbon metabolism genes and viral community temperateness.

Figure 3: Pathway map of changes in the frequency of central carbon metabolism genes across the lytic to temperate spectrum.

Figure 4: Correlations between viral community temperateness and central carbon gene frequency across pathways and gene function.

Figure 5: Schematic model incorporating viral metabolic effects on resilience of healthy coral reefs and exacerbation of reef degradation.

List of Supplementary Tables and Figures

Supplementary Table 1: Summary of samples analyzed, including sample accession numbers, the total number of base pairs, reads, and locations of viral metagenomes.

Supplementary Table 2: Parameters and values used in the qualitative ecosystem model.

Supplementary Table 3: The frequency of photosynthesis genes across the lytic-temperate spectrum.

Supplementary Figure 1: Temperate viral communities are more cell-like, and have higher gene diversity and evenness, but not richness.

Supplementary Figure 2: Bootstrapped distribution of ρ_s from 1,000 iterations correlating the frequency of central carbon metabolism genes with viral community temperateness.

Significance (114 words)

Coral reefs are collapsing worldwide, exacerbated by "microbialization," where algae-fueled bacteria overgrow corals. Viruses that infect these bacteria can suppress this process through lysis, but on degraded reefs they often switch to nonlethal temperate lifestyles, accelerating decline. Here we show that similar shifts occur in virus-encoded metabolism. On healthy reefs, lytic viruses carry genes that drain host metabolites to fuel virus production, which likely enhances infection and lysis rates and limits bacterial overgrowth. On degraded reefs, temperate viruses encode reactions that expand host metabolite pools, supporting bacterial proliferation. Thus, viral metabolism can either reinforce reef resilience or exacerbate collapse, making it a hidden driver of ecosystem fate and a potential target for conservation strategies.

Abstract (235 words)

Coral reefs are declining globally due in part to bacterial overgrowth, a process known as microbialization. However, the role of bacteriophages that may inhibit microbialization by infecting and killing these bacteria remains poorly understood, especially their metabolic impacts on bacterial proliferation. To address this, we analyzed central carbon metabolism gene frequencies in viral communities from healthy (lytic-dominated) and degraded (temperate-dominated) Central Pacific coral reefs. We found that viral metabolism shifted broadly from being dominated by metabolism that builds up pools of central intermediates on degraded reefs dominated by temperate viral infection ('anaplerotic' reactions) to metabolism that consumes these pools to prioritize production of metabolic precursors for virion construction on healthy reefs dominated by lytic infection ('cataplerotic' reactions). This switch was shown by the over-representation of Entner-Doudoroff (ED) glycolysis genes on degraded, temperate-dominated reefs and of pentose phosphate pathway (PPP) and reductive tricarboxylic acid cycle (TCA) genes on healthy, lytic-dominated reefs. As a result of this metabolic dichotomy, our qualitative compartment modeling revealed two distinct ecosystem states: (i) healthy reefs, where lytic viral metabolism enhances viral production and suppresses bacterial overgrowth, and (ii) degraded reefs, where temperate viral metabolism accelerates bacterial proliferation. Because viral switching between lytic and temperate lifestyles is a known function of host physiological state, these findings position viral metabolism as both a driver of reef decline and a conservation lever, with metabolically mediated 're-viralization' offering a novel strategy to restore reef resilience.

115 **Introduction** (704 words)

116 Ecosystem overgrowth by microbes, a process known as microbialization, is a
117 major threat to coral reefs worldwide[1–3]. Microbialized reefs are subject to a
118 positive feedback loop in which proliferating algae generate excess dissolved
119 organic carbon (i.e., sugar) that fuels the growth of increasingly pathogenic and
120 copiotrophic microbes that thrive in nutrient-rich environments[1,4,5]. This process
121 exacerbates coral diseases and clears space for further algal growth[2,6–8].

122 Bacterial metabolism on degraded coral reefs is directed towards high-
123 throughput rather than efficient carbohydrate utilization[1,9]. For instance, while
124 bacterial metabolism on healthy reefs is dominated by genes for the efficient
125 but multi-step Embden-Meyerhof-Parnas (EMP) pathway, degraded reefs exhibit
126 greater representation of genes for the inefficient but short Entner-Doudoroff
127 (ED) glycolysis pathway [1,10–12]. This shift on degraded reefs enable bacteria to
128 readily exploit ecosystem organic carbon enrichment to build up cellular
129 stockpiles of central metabolites like glyceraldehyde-3-phopshate (G3P) and
130 pyruvate ('anaplerotic' reactions) as well as use those central metabolite pools
131 to produce cellular energy such as ATP, reductants like NADH, and amino and
132 nucleic acid biosynthetic precursors required for bacterial over-proliferation
133 ('cataplerotic' reactions)[1,7,11].

134 Viral predation could, in principle, preclude microbialization by killing
135 proliferating microbes, as lytic infection and lysis rates are predicted by
136 established predator-prey models to rise with host densities and growth rates[13–
137 16]. However, viral communities switch from lytic to temperate infection during
138 eutrophication and microbialization[14]. This transition towards non-lethal,
139 temperate infection can facilitate further increases in microbial biomass due to
140 suppressed lysis[14,17]. Further, temperate viral communities encode higher
141 frequencies of pathogenicity genes that could protect bacteria from
142 consumption by eukaryotic grazers[14,18–20]. These genes could facilitate

143 microbialization by limiting protist predation, the major non-viral predation guild
144 in the ocean[21,22]. Altogether, rather than controlling bacterial populations,
145 viruses may form a second 'Temperate Ratchet' feedback loop that traps
146 ecosystems in persistent microbialization through suppressed lysis rates and
147 protist grazing on pathogenic copiotrophs[14,23].

148 In addition to these population-level effects, viruses may also exert gene-level
149 effects on microbialization by reshaping bacterial metabolism. Viruses shuttle a
150 broad array of metabolic genes between hosts via horizontal gene transfer,
151 thereby altering bacterial metabolism and ecology[24–27]. These include central
152 carbon metabolism genes implicated in the metabolic switching of bacterial
153 communities on microbialized reefs, such as the pentose phosphate pathway
154 (PPP) and the ED and EMP glycolysis pathways[1,28]. In lytic viruses, these pathways
155 support virion synthesis by converting general cellular metabolic pools like G3P
156 and pyruvate to specialized metabolic precursors (i.e., they are cataplerotic
157 reactions). For example, the PPP provides nucleic acid and amino acid
158 precursors, whereas EMP generates cellular energy like ATP and NADH[27,29,30].
159 However, these genes can also be co-opted by bacteria during infection. As a
160 result, while viral metabolic genes can combat microbialization by promoting
161 the production of lytic viruses that would suppress bacterial abundance, they
162 are also capable of exacerbating reef decline by enhancing bacterial
163 proliferation. Together, these processes introduce a novel viral-mediated
164 metabolic mechanism of reef decline or resilience beyond lytic-to-lysogenic
165 switching.

166 However, the role of viral-encoded metabolic genes in coral reef
167 microbialization remains unexplored. To address this gap, we leveraged 19
168 metagenomes of virus-like particles (VLPs; viromes) used in several prior
169 publications[11,14,31], from Pacific coral reefs spanning a gradient from healthy to
170 degraded states and from lytic to temperate infection dominance, to

171 characterize changes in the frequencies of viral metabolic genes across a viral
172 lifestyle spectrum. We found that temperate viral communities were enriched in
173 anaplerotic central carbon metabolism genes, particularly those associated
174 with copiotrophic growth like Entner-Doudoroff glycolysis and the generation of
175 central metabolite pools that can be used for diverse cellular processes[32]. Lytic
176 communities had higher levels of cataplerotic non-oxidative pentose phosphate
177 pathway genes and oxidoreductases that generate specialized metabolic
178 precursors, cellular energy and redox potential. Incorporating our findings into a
179 conceptual model revealed that lytic viral metabolism can enhance viral
180 production and microbial surveillance on healthy reefs ("viralization")[33], while
181 temperate viral metabolism may accelerate microbialization in degraded
182 systems. These findings implicate viral metabolism in feedback loops that either
183 enhance reef resilience or exacerbate decline. Because viral lifestyle switching is
184 a known function of cellular physiological state, with elevated nutrient
185 availability driving non-lethal temperate infection, while nutrient limitation
186 promotes lytic infection, our work suggests that metabolic management, such
187 as limiting nutrient inputs, could promote rapid recovery of degraded reefs.

188 **Methods** (1764 words)

189 *Metagenome sampling and processing:* Metagenomes were sampled from
190 virus-like particles (VLPs) from coral reefs across the central Pacific Ocean (n =
191 19; see **Supplementary Table 1** for sample details) and samples processed as
192 described previously[14,34]. For each viral metagenome, approximately 60-100 L of
193 seawater were pumped from the reef surface into acid-washed, triple-rinsed
194 low-density polyethylene bags and concentrated to < 500 mL using a 100 kDa
195 tangential flow filter. Concentrates were then 0.45 µm-filtered to remove
196 bacteria and 0.5 % final concentration chloroform was added to destroy any
197 residual cells and extracellular vesicles[35]. Samples were stored at 4 °C until
198 subsequent processing. The presence of concentrated VLPs was confirmed by
199 epifluorescence microscopy of Sybr Gold stained viruses on anodisc filters[34].

200 VLPs were purified from concentrates using a cesium chloride step gradient
201 approach[14,34,36]. The absence of cells in step gradient outputs was confirmed by
202 microscopy. Purified samples were then DNAse I-treated at 37 °C for 2 hours and
203 denatured at 65 °C for 15 minutes to remove extra-virion free DNA (peDNA;
204 protected environmental DNA)[37]. Viral DNA was extracted using the
205 formamide/chloroform isoamyl alcohol technique[14,34,36]. The absence of
206 contaminating host DNA in all samples was confirmed by the lack of PCR
207 amplification of the universal 16S rDNA gene using primers 27F (AGA GTT TGA
208 TCC TGG CTC AG) and 1492R (TAC GGY TAC CTT GTT ACG ACT T)[14,34,36]. Note
209 that our analysis is based on correlations across many samples, minimizing the
210 impact of any contamination on our findings. VLP DNA was amplified using the
211 Linker Amplified Sequencing Library approach[19] prior to sequencing on an
212 Illumina MiSeq platform.

213 *Bioinformatic processing:* Low-quality reads < 100 bp in length and with mean
214 PHRED quality scores of < 25 were excluded using Prinseq[38]. Samples were then
215 dereplicated with TagCleaner[39], human contaminants were removed using

216 DeconSeq[40], and sequences were posted to MG-RAST (www.mg-rast.org; see
217 Data Availability section). Accession numbers and summary statistics for the viral
218 metagenomes used in this paper are shown in **Supplementary Table 1**.

219 *Annotating metagenomes:* Viral metagenomes were annotated by DIAMOND
220 alignment against the SEED subsystems database on MG-RAST v4 using the
221 default MG-RAST parameters as a very commonly used balance of accuracy
222 and specificity[41]: e-value = -5 (annotated in MG-RAST as e-value = 5), 60 %
223 identity, > 15 base length, a minimum abundance of 1, and all analyses
224 conducted using representative hits (February 2020)[14,42]. Level 1 Gene
225 categories with average frequencies below 0.5 % were omitted. Temperateness
226 of each viral metagenome was assessed as the frequency of genes annotated
227 in the Level 3 SEED category of "Phage_integration_and_excision" (i.e., how
228 common genes involved in integration and excision were in each
229 metagenome)[14]. The frequency of genes in high-order classification (e.g., SEED
230 level 1 with categories shown in **Figure 1**) was calculated by summing the
231 frequency of the genes making up each category. All analyses were normalized
232 to account for different sequencing depth between samples. This was done by
233 calculating gene frequency as the number of hits to a given gene divided by all
234 known genes in that sample ("percent known")[15], making all analyses
235 comparable and unaffected by the effects of varied sequencing depth
236 between samples.

237 *Pathway annotation:* Pathway visualizations were guided by KEGG maps
238 (www.genome.jp/), pathway-specific Wikipedia pages (www.wikipedia.org/),
239 and enzyme Wikigenes entries (www.wikigenes.org/). Pathway maps were
240 drawn using EC Number names of each enzyme (**Table 1**).

241 *Anaplerotic and cataplerotic gene categorization:* Genes were categorized
242 based on whether they (i) generated central metabolite pools like
243 glyeraldehyde-3-phopshate (G3P) and pyruvate ('anaplerotic' or 'filling up'

244 reactions) that are flexibly used in multiple pathways by cells, or (ii) used these
245 central metabolite pools to generate cellular energy or metabolic precursor
246 products that are used for specific purposes (i.e., the products are 'used'
247 metabolically; known together as 'cataplerotic' or 'drawing down' reactions),
248 or (iii) were neither anaplerotic nor cataplerotic ('neither'). Note that although
249 anaplerotic and cataplerotic reactions often refer to steps in the TCA, we are
250 using the term more generally here[32].

251 *Statistical analyses:* The correlation between gene frequency, either at a Level 1
252 SEED category or individual gene level, and viral community temperateness
253 were assessed using Spearman's Rho (ρ_s), a non-parametric rank-based
254 measure of how monotonic the relationship between x- and y-values is (i.e., it is
255 a non-parametric correlation coefficient). For supplementary diversity and
256 photosynthesis gene analyses we estimated ρ_s using the R cor.test() function
257 with exact = FALSE to avoid ties. For our main analyses shown in **Table 1** and in
258 **Figures 1**, **2**, **3**, and **4**, we estimated ρ_s values using the stat.spearmanr() function
259 in the Python scipy.stats package with bootstrapping to ensure robust median ρ_s
260 assessment over 1000 iterations of bootstrapping with replacement (see
261 **Supplementary Figure 2** for resulting distributions for central carbon metabolism
262 genes). Confidence intervals of the median were assessed as the values
263 corresponding to the 2.5th and 97.5th percentiles of the median values
264 obtained from bootstrapping (95 % CI). For clarity, 95 % confidence intervals are
265 listed in square brackets, as ρ_s [95 % CI minimum, 95 % CI maximum].
266 Bootstrapping code can be found at
267 https://github.com/hopefulmonstersucla/viral-metabolism/tree/main/code.
268 Note that correlations are significant at $p < 0.05$ when 95% bootstrap
269 confidence intervals exclude zero, equivalent to classical null hypothesis testing.

270 Diversity metrics were assessed using the R vegan package, with the diversity()
271 command used for Shannon diversity (natural log-transformed; H'). Median ρ_s at

the pathway level were calculated as the median value of all of the ρ_s values for each enzyme in the pathway (i.e., they are a simple overall median).

Qualitative model: We created a conceptual model to demonstrate qualitative trends in bacterial, viral, coral, and algae abundance stemming from the changes in viral metabolism found here (**Figure 5**). Note that this model is not intended to be quantitative and was designed aid our understanding of trends in organismal abundance in response to the incorporation of viral metabolic capacity. Parameter values were implemented as high or low relative values to reflect known processes on healthy and degraded reefs (**Supplementary Table 2** for parameter values). For example, high rates of disease[8,43] and bacterial metabolism[1] were used in degraded coral reef simulations, while high lysis rates were used in healthy systems[14,17].

Bacterial, viral, coral, and algae populations were initialized at 0.5 arbitrary units. The model was implemented using an iterative loop over six iterations (i.e., time in arbitrary units). This number of iterations was chosen as a balance of having enough iterations to see qualitative population trends, but without the need to make a more complicated model to generate long-term dynamics. At the beginning of each time step, new abundance values for each species (B_{new}, C_{new}, V_{new}) except algae were calculated based on the previous values (A_{new}). These updated values were applied at the end of each time step. Algae abundance was calculated last, occupying any remaining share of the benthos not occupied by coral. Once a population reached or fell below zero, it was excluded from further dynamics and not allowed to re-enter the ecosystem. Code can be found at https://github.com/hopefulmonstersucla/viral-metabolism/tree/main/code.

For the 'no viruses' model shown in **Figures 5a** and **5d**, we used the following equations, where terms with changed parameter values between **Figures 5a** and **5d** are in bold (see **Supplementary Table 2**):

300 $B_{new} = B + a * A + \mathbf{m * B}$ Equation 1

301 $C_{new} = C + c * C - i * A - \mathbf{d * B}$ Equation 2

302 $A_{new} = 1 - C_{new}$ Equation 3

303 In **Equation 1**, bacteria (B) proliferate due to carbon provided by algae, with
304 carbon supply itself a product of algal population (A) as well as the rate of
305 delivery (a). To make the model as conservative as possible, we did not vary the
306 rate of carbon delivered to bacteria by the algae, although it likely is higher on
307 degraded reefs and enhances bacterial grow more than shown by the model[10].
308 Bacterial proliferation is also enhanced by metabolic changes (m) reinforced by
309 bacterial population size on degraded reefs[1]. Note that, in the absence of
310 viruses the bacteria have no loss processes, including natural mortality, even
311 though their proliferation may be constrained by a lack of algae to support
312 growth.

313 In **Equation 2**, coral populations (C) proliferate as a product of coral population
314 size and growth rate (c). Coral growth is limited by algal population size and
315 allelochemical inhibition (i)[44] as well as by bacterial pathogenicity causing coral
316 disease (d)[8,45]. To make the model as conservative as possible, we did not alter
317 the direct inhibitory effect of algae on coral across healthy and degraded reefs,
318 although it is enhanced on unhealthy reefs[44,45].

319 In **Equation 3**, algal population size (A) is solved in the last step of each iteration
320 as the remainder of the benthos not occupied by coral (1 – C) to account for
321 the fact that the benthos is a finite space.

322 Note that **Equations 2** and **3** are used for all iterations of the model with or
323 without viral lysis and metabolism.

For the 'with lytic viruses' model shown in **Figures 5b** and **5e** we used the following equations, with bold terms reflecting varied parameter values and with new terms compared to **Equations 1** and **Equation 2** underlined:

$$B_{new} = B + a * A + \mathbf{m * B} \underline{\mathbf{- k * V}} \qquad \text{Equation 4}$$

$$\underline{V_{new} = V + \mathbf{k * B}} \qquad \text{Equation 5}$$

Building on **Equation 1**, lytic viruses are introduced in **Equation 4** as a mortality term for bacteria as an outcome of viral population size (V) and lysis rate (k).

A viral population (V) is added to the model in **Equation 5**, where viruses proliferate at burst size (k) from lysis if bacteria. Note that k changes between healthy and degraded reef scenarios, consistent with Piggyback-the-Winner dynamics suppressing lysis on degraded reefs[14].

For the 'with viral lysis and metabolism' model shown in **Figures 5c** and **5f** we used the following equations, with bold terms reflecting varied parameter values and with new terms compared to **Equations 4** and **5** underlined:

$$B_{new} = B + a * A + \mathbf{m * B} - \mathbf{k * V} \underline{\mathbf{+ t * V}} \qquad \text{Equation 6}$$

$$V_{new} = V + \mathbf{k * B} \underline{\mathbf{+ l * V}} \qquad \text{Equation 7}$$

This model builds on **Equation 4** by adding viral metabolic function (t) that enhances bacterial proliferation in degraded reef scenarios associated with temperate Piggyback-the-Winner dynamics in **Equation 6**[14]. **Equation 7** builds on **Equation 5** by adding lytic functions that enhance virion production in healthy reefs (l).

345 **Results** (1724 words)

346 *Hallmarks of viral temperateness:* To assess how viral metabolism across the lytic-
347 temperate spectrum could affect coral reefs, we examined how the fraction of
348 sequenced reads that mapped to known genes in broad metabolic categories
349 (SEED Database Level 1 annotation) changed with community temperateness.
350 Building on prior work[14], we used the frequency of integrase and excisionase
351 genes as a proxy for community temperateness (i.e., hallmarks of
352 temperateness) in viral communities across the Central Pacific Ocean
353 (**Supplementary Table 1**). As a measure of how consistently or monotonously
354 gene frequency and sample temperateness covary, Spearman Rho (ρ_s) values
355 reflect the strength and sign of their correlation. In this analysis, temperate-
356 associated genes have positive correlations ($\rho_s > 0$) while lytic-associated genes
357 have negative correlations ($\rho_s < 0$. For clarity, 95 % confidence intervals are
358 listed in square brackets as ρ_s [95 % CI minimum, 95 % CI maximum], and
359 correlations where the confidence intervals exclude zero are significant at the p
360 < 0.05 level.

361 Gene names and corresponding pathways, EC numbers, median ρ_s and 95 %
362 CIs, gene category (anaplerotic vs cataplerotic), and reports of the gene in
363 viruses are shown in **Table 1**. **Figure 1** and **Figure 2** display the sample-level
364 patterns of temperateness vs gene frequency in all Level 1 SEED categories and
365 in central carbon metabolism functions, respectively. The correlations shown in
366 **Figure 2** are represented in a metabolic pathway map in **Figure 3** and analyzed
367 according to **Table 1** categories in **Figure 4**. Finally, the implications of our
368 central findings are incorporated into a schematic ecosystem model shown in
369 **Figure 5**.

370 *Temperate viral communities are enriched in metabolic genes:* The frequency of
371 genes in the Phages, Prophages, Transposable Elements, and Plasmids category
372 declined with increasing temperateness of viral communities (**Figure 1**; ρ_s = -0.81

373 [-0.95, -0.58]). In contrast, the frequency and diversity of 'bacterial' metabolic
374 genes that encode known cellular functions increased in temperate viral
375 communities (**Supplementary Figure 1**; ρ_s = 0.63 and 0.81, respectively; c.f.,
376 genetic diversity declines with temperateness when unknown genes are
377 included[14]). Altogether, this analysis indicates that temperate viral communities
378 are more metabolically similar to bacteria than are lytic communities.

379 *Functional homologues as viral lifestyle markers:* Analogous to taxonomic
380 markers in cells, where the prevalence of class I and class II homologues of
381 fructose bisphosphate aldolase EC4.1.2.13 genes relates to bacterial
382 taxonomy[46], the divergent correlations in these genes across a viral
383 temperateness spectrum may reflect viral life strategies (EC 4.1.2.13 I ρ_s = -0.65 [-
384 0.86, 0.33] while EC4.1.2.13 II ρ_s = 0.56 [-0.18, 0.83]; see **Table 1** for summary
385 statistics).

386 *Photosynthesis genes in lytic communities:* The decline in 'Phages, Prophages,
387 Transposable Elements, and Plasmid' genes from ~ 50 % of the known genes in
388 lytic viromes to ~ 5 % in temperate viromes caused the gene frequency in almost
389 all other categories to increase (as total gene frequencies sum to 100 %; 17 of 22
390 categories had ρ_s > 0.5; **Figure 1**). A notable exception is Photosynthesis genes:
391 these had higher frequencies in lytic communities vs. temperate communities in
392 the Level 1 analysis (ρ_s = -0.78 [-0.92, -0.53]; **Figure 1**). Photosynthesis genes,
393 including rhodopsins, were also lytic-associated at the individual-gene level,
394 where 16 out of 20 photosynthesis genes had negative ρ_s values (**Supplementary**
395 **Table 3**). Finally, photosynthesis-related electron transport (Pet) genes that
396 couple Photosystems II and I are absent from the viromes (**Supplementary Table**
397 **3**).

398 *Carbohydrate metabolism genes:* Given the high prevalence of carbohydrate
399 genes in the viromes, their elevated frequency in temperate communities
400 (**Figure 1;** ρ_s > 0), and their ecological importance, we next focused on genes

401 comprising central carbon metabolism[26,27]: Embden-Meyerhof-Parnas (EMP) and
402 Entner-Doudoroff (ED) glycolysis pathways, the pentose phosphate pathway
403 (PPP) and the Tricarboxylic Acid Cycle (TCA; **Figure 2**). Note that for this and
404 subsequent analyses we retained only sequences with hits to SEED database
405 entries with high-confidence Enzyme Commission (EC) annotations[47].

406 *Entner-Doudoroff genes are enriched in temperate viromes:* Few patterns were
407 readily apparent from the ρ_s values for genes in each pathway (**Figure 2;**
408 **Supplementary Figure 2**). When viewed as a pathway map, though, the ED
409 pathway was more clearly enriched in temperate viral communities (i.e., the red
410 arrows running through the center of **Figure 3**). This map identified the ED
411 pathway as the only pathway that changed consistently across the lytic-
412 temperate spectrum (**Figure 4a**), and was exclusively over-represented in
413 temperate viral communities (i.e., $\rho_s > 0$; EC 1.1.1.49 $\rho_s = 0.26$ [-0.24, 0.68],
414 EC3.1.1.31 $\rho_s = 0.43$ [0.03, 0.77], EC4.1.2.14 $\rho_s = 0.67$ [0.36, 0.90], and EC4.2.1.12 ρ_s
415 $= 0.71$ [0.47, 0.89]). Altogether, this gave the ED pathway an overall median $\rho_s =$
416 0.55 in contrast to overall median $\rho_s = 0.03$ for EMP glycolysis, $\rho_s = 0.175$ for
417 gluconeogenesis (GNG), $\rho_s = 0.03$ for the PPP, and $\rho_s = -0.10$ for the TCA (see
418 **Figure 4a**).

419 *Anaplerotic temperate metabolism:* Given the role of ED glycolysis in generating
420 central metabolite pools for use in diverse pathways (i.e., ED is an anaplerotic
421 pathway), we investigated whether temperate viral communities were enriched
422 in anaplerotic genes more generally (see **Table 1** for a list of anaplerotic and
423 cataplerotic genes)[32]. Temperate viral communities were, indeed, enriched in
424 anaplerotic genes, with an overall median $\rho_s = 0.44$ for anaplerotic reactions
425 and only one gene even weakly lytic associated (6-phosphogluconate
426 dehydrogenase EC 1.1.1.44 from the PPP; $\rho_s = -0.06$ [-0.54, 0.45]; **Figure 4b**).

427 *Amino acid precursor genes are enriched in lytic viromes:* In contrast to the ED-
428 enrichment of temperate communities, the pathway map does not show many

429 areas of contiguous lytic-associated genes (**Figure 3**). However, the enrichment
430 of non-oxidative PPP genes in lytic communities, especially transaldolase EC
431 2.2.1.2 (ρ_s = -0.49 [-0.87, 0.02]). This enzyme consumes the central metabolite
432 pool of glutaraldehyde-3-phosphate (G3P) to produce fructose 6-phosphate
433 and erythrose 4-phosphate. Given that other fructose-6-phosphate producing
434 genes are not similarly enriched in lytic communities (e.g., EC 2.2.1.1 in the PPP
435 ρ_s = -0.08 [-0.52, 0.35], EC5.3.1.9 in EMP ρ_s = 0.45 [0.12, 0.73], and EC3.1.3.11 in
436 gluconeogenesis ρ_s = 0.24 [-0.20, 0.66]), this suggests that the primary outcome
437 of the non-oxidative PPP in lytic viral communities is the cataplerotic
438 consumption of G3P for the generation of erythrose-4-phosphate, a precursor
439 for amino acid biosynthesis[48].

440 *Redox genes are over-represented in lytic communities:* Given this cataplerotic
441 focus in lytic communities, we investigated whether lytic communities were
442 more strongly associated with individual cataplerotic reactions regardless of
443 pathway rather than with whole pathways. Focusing on the distribution of
444 anabolic redox steps across all the central carbon metabolism pathways, we
445 found that NADPH-generating reactions were not consistently associated with
446 either lytic or temperate communities (EC1.1.1.44 ρ_s = -0.06, EC1.1.1.42 ρ_s = -0.19,
447 and EC1.1.1.49 ρ_s = 0.26, giving a median ρ_s = -0.06). In contrast, NADH-
448 producing oxidoreductase genes were universally over-represented in lytic
449 communities (i.e., all $\rho_s < 0$; median ρ_s = -0.13 across all NADH-producing
450 reactions from EC1.1.1.37 ρ_s = -0.19 [-0.61, 0.29], EC1.1.1.41 ρ_s = -0.13 [-0.54, 0.34],
451 EC1.2.1.12 ρ_s = -0.20 [-0.60, 0.26], EC1.2.4.1 ρ_s = -0.12 [-0.60, 0.36], EC1.2.4.2 ρ_s = -
452 0.10 [-0.59, 0.42]; **Table 1**; **Figures 2**, **3,** and **4**). This included all redox genes in the
453 TCA being lytic associated (i.e., $\rho_s < 0$, with an overall median ρ_s = -0.13) in
454 contrast to the other, non-oxidoreductase genes which had a median ρ_s = 0.15,
455 highlighting the specific overrepresentation of redox genes in lytic communities
456 (**Figure 4a**).

457 *Cataplerotic lytic metabolism:* Given the association between lytic communities
458 and cataplerotic reactions observed in the PPP and the TCA, we then
459 investigated whether lytic communities are broadly enriched in cataplerotic
460 genes. We observed that the overall median ρ_s of cataplerotic reactions was -
461 0.125 (i.e., these genes were enriched in lytic communities) compared to ρ_s =
462 0.44 and ρ_s = 0.11 for anaplerotic reactions and reactions that are neither
463 cataplerotic nor anaplerotic, respectively. This result highlights the association
464 between lytic viral communities and cataplerotic metabolism.

465 *Implications for Healthy Coral Reefs:* To qualitatively describe the ecosystem
466 effects of viral metabolism, we constructed a schematic model of algal-
467 bacterial-viral-coral interactions, with all population sizes measured in illustrative
468 arbitrary units (**Figure 5**). Parameterizing the model to healthy reef values (**Figure**
469 **5a**; note that parameterization of the healthy reef scenario largely insulates
470 coral from the effects of bacterial overgrowth due to the small d value used;
471 see **Supplementary Table 2** for parameters and values)[1,8,9,14,43], the system
472 became coral-dominated by t = 5, with coral-bacterial coexistence (coral and
473 bacteria had increased from 0.5 a.u. initial values to 1.0 a.u. and 0.89 a.u.,
474 respectively, by t = 6). While the addition of viral lysis (**Figure 5b**) did not
475 markedly change coral or algal dynamics, it led to the extinction of bacteria by
476 t = 6 and to an ecosystem dominated by coral and viruses (coral and viruses
477 had increased from 0.5 a.u. to 1.0 a.u. and 0.97 a.u., respectively, by the end of
478 the simulation). Finally, adding in viral metabolism led to an earlier extinction of
479 bacteria (by t = 5) and enhanced viral population size (viruses were 2.29 a.u. by
480 t = 6), although coral and algal population dynamics were unaffected (**Figure**
481 **5c**). Altogether, the model recaptured the coral-dominated status of healthy
482 coral reefs and showed that viral metabolism likely exerts a profound negative
483 effect on bacterial populations and a strongly positive effect on viral
484 populations on healthy reefs.

485 *Implications for Degraded Coral Reefs:* In contrast to healthy systems, our model
486 suggests that degraded coral reefs would be overgrown with algae rather than
487 coral (**Figure 5**). Note that the parameterization of the degraded reef scenarios
488 leads to enhanced deleterious bacterial effects on coral health. Coral went
489 extinct by t = 5 in the degraded scenarios without viruses and with viral lysis only
490 (**Figure 5d and e**), as algal overgrew the benthos and bacterial proliferated to
491 levels much higher than in any of the healthy scenarios (B = 2.75 a.u. and 2.64
492 a.u. in the no virus and lysis-only models, respectively, by t = 6). In contrast to
493 bacteria, viral populations did not proliferate markedly in the viral-lysis model,
494 increasing from 0.5 a.u. to only 0.64 a.u. by t = 6 (**Figure 5e**). Adding in viral
495 metabolism that enhanced bacterial proliferation (t) allowed bacteria to
496 proliferate even further (reaching 3.80 a.u.), supporting a modest rise in viruses
497 (to 0.75 a.u.), and driving the coral to extinction sooner (by t = 4; **Figure 5f**).
498 Altogether, our qualitative model suggests that viral metabolism supporting
499 bacterial proliferation can enhance microbial overgrowth of reefs and promote
500 shifts towards algal dominance of the benthos.

501 **Discussion** (551 words)

502 The role of microbial overgrowth in coral reef decline is well established[1–3,8]. It is
503 further intensified by shifts in bacterial metabolism and viral lifestyles that
504 promote bacterial proliferation[14,17]. Here, we show that this process is further
505 exacerbated by viral-encoded metabolic genes, whereas healthy ecosystems
506 may be protected by viral lysis and metabolic genes that enhance virion
507 production. Because temperate viral infection is tightly linked to host physiology
508 and environmental conditions such as nutrient availability[14,49,50], targeting
509 bacterial metabolic states through manipulation of nutrients could enable a shift
510 in viral effects from degradative to protective, presenting a promising new
511 conservation strategy.

512 Viruses become increasingly temperate on degraded reefs, following
513 Piggyback-the-Winner (PtW) dynamics[14,23], in which abundant, rapidly
514 proliferating bacterial hosts select for non-lethal, lysogenic infection. This switch
515 in viral lifestyle suspends the top-down control exerted by lytic viruses, allowing
516 bacterial populations to expand unchecked by lethal infection[14,50]. Temperate
517 infection not reduces lysis but also promotes horizontal gene transfer of
518 pathogenicity genes[51], which can help bacteria evade predation by eukaryotic
519 grazers and potentially compromise coral health[14,23]. This forms a positive
520 feedback loop wherein bacterial growth triggers viral lifestyle switching, which in
521 turn facilitates further bacterial growth, establishing a 'Temperate Ratchet'[23]
522 that locks ecosystems into ever-exacerbating bacterial overgrowth and coral
523 disease[14]. Worse, here we show that the temperate viruses on degraded reefs
524 also harbor metabolic genes, such as those for Entner-Doudoroff glycolysis, that
525 can directly support bacterial proliferation and overgrowth of reefs[1], thereby
526 enhancing the Temperate Ratchet[23].

527 Healthy reefs, in contrast, appear to be guarded by lytic viruses. Lytic infection
528 rates are driven by virus-host predator-prey encounter frequencies that are the
529 outcome of host and viral abundances[13–15]. As a result, as bacterial populations
530 grow, so should lytic infections and lysis, precluding bacterial overgrowth[14,17].
531 Further, the viral communities on healthy reefs do not harbor the high frequency
532 of pathogenicity genes seen on degraded reefs, meaning that grazing and
533 coral health are not being hindered by viral-encoded genes, which also helps
534 to keep bacterial densities low[8]. Here we show that lytic viral communities on
535 healthy reefs are enriched in metabolic genes associated with efficient energy
536 production and biosynthesis, such as those for the Embden-Meyerhof-Parnas
537 glycolysis pathway[1,10] and oxidoreductases involved in ATP generation and
538 NADH reduction[52]. These metabolic features support robust virion production
539 that can support reef 'viralization' through high viral abundances and high rates
540 of virus-host encounters, infection, and lysis. In this way, lytic viral metabolism
541 and reef viralization acts as a counterbalance to the Temperate Ratchet,
542 helping to stabilize healthy reef ecosystems[33].

543 Viral metabolism associated with the lytic-to-temperate shift likely exacerbates
544 coral reef decline, as shown here. Building on ecosystem-scale processes like
545 viral lifestyle switching[14,17], the metabolic capacity of temperate and lytic viruses
546 can further drive reefs into two stable states: healthy reefs protected by
547 metabolically enhanced lytic control of bacteria, and degraded reefs
548 ratcheted into persistent microbialization under temperate infection and
549 metabolism. Ultimately, degraded coral reefs experience a metabolic disorder,
550 where excess nutrients trigger ecosystem-scale dysregulation through microbial
551 and viral lifestyle and metabolic switching[1–3,7]. However, the physiological basis
552 of this switch also suggests that conservation measures targeting nutrient supply
553 could undercut copiotrophic bacterial and viral metabolism[4,10,11]. Our findings
554 suggest that doing so could lead to a 're-viralization' of the reef system,

555 harnessing viral metabolic and lifestyle switching to enhance reef restoration
556 and resilience.

557 **Data Availability**

558 Viral metagenomes can be found on MG-RAST under the accession numbers
559 4683670.3, 4683674.3, 4683677.3, 4683680.3, 4683683.3, 4683684.3, 4683686.3,
560 4683703.3, 4683704.3, 4683712.3, 4683718.3, 4683720.3, 4683731.3, 4683733.3,
561 4683745.3, 4683746.3, and 4683747.3 (see **Supplementary Table 1** for library data
562 summaries; www.mg-rast.org). Fasta files for each sample, statistical and
563 modeling code, and annotations and simulations data can be found at
564 https://github.com/hopefulmonstersucla/viral-metabolism.

565

Acknowledgments

This work was supported by a BIG Summer stipend from Simons Foundation (awarded to Alexander Hoffmann for CU and NY) as well as by NSF Award OCE-2201645 to BK that provided Hopeful Monsters Summer stipends to JK, MK, GD, NF, EG, AK, and IT. LWK was supported by NSF award OCE-2118617. RAE was supported by an award from the NIH NIDDK RC2DK116713, an award from the Australian Research Council DP220102915, and an award from the Gordon and Betty Moore Foundation number 9871 (Perpetual Viral Origins). JG was supported by NSF Biology Integration Institute award 2119968. ML was supported by an NSF Postdoctoral Research Fellowship in Biology award 2209377. The authors would like to thank the captain, crew, and staff of the *NOAAS Hi'ialakai* (R 334) and National Oceanic and Atmospheric Administration (NOAA) shore support, as well as the members of the Pacific Reef Assessment and Monitoring Program of NOAA's National Coral Reef Monitoring Program.

580 **References**

581 1. Haas, A. F. *et al.* Global microbialization of coral reefs. *Nat. Microbiol.* **1**, 1–7
582 (2016).
583 2. Kelly, L. W., Haas, A. F., Nelson, C. E. & Rohwer, F. Microbialization in coral
584 reefs: insights into the mechanisms and consequences of a changing
585 benthos. *mBio* **5**, e00080-14 (2014).
586 3. McDole, T. *et al.* Assessing Coral Reefs on a Pacific-Wide Scale Using the
587 Microbialization Score. *PLoS ONE* **7**, e43233 (2012).
588 4. Nelson, C. E., Wegley Kelly, L. & Haas, A. F. Microbial interactions with
589 dissolved organic matter are central to coral reef ecosystem function and
590 resilience. *Annu. Rev. Mar. Sci.* **15**, 431–460 (2023).
591 5. Haas, A. F. *et al.* Influence of coral and algal exudates on microbially
592 mediated reef metabolism. *PeerJ* **1**, e108 (2013).
593 6. McDole Somera, T. *et al.* Energetic differences between bacterioplankton
594 trophic groups and coral reef resistance. *Proc. R. Soc. B Biol. Sci.* **283**,
595 20160467 (2016).
596 7. Smith, J. E. *et al.* Indirect effects of algae on coral: algae-mediated,
597 microbe-induced coral mortality. *Ecol. Lett.* **9**, 835–845 (2006).
598 8. Barott, K. L. & Rohwer, F. L. Unseen players shape benthic competition on
599 coral reefs. *Trends Microbiol.* **20**, 621–628 (2012).
600 9. Roach, T. N. *et al.* Microbial bioenergetics of coral-algal interactions. *PeerJ* **5**,
601 e3423 (2017).
602 10. Nelson, C. E. *et al.* Coral and macroalgal exudates vary in neutral sugar
603 composition and differentially enrich reef bacterioplankton lineages. *ISME J.*
604 **7**, 962–979 (2013).
605 11. Silveira, C. B. *et al.* Microbial processes driving coral reef organic carbon
606 flow. *FEMS Microbiol. Rev.* **41**, 575–595 (2017).
607 12. Flamholz, A., Noor, E., Bar-Even, A., Liebermeister, W. & Milo, R. Glycolytic
608 strategy as a tradeoff between energy yield and protein cost. *Proc. Natl.*
609 *Acad. Sci.* **110**, 10039–10044 (2013).
610 13. Thingstad, T. F. Elements of a theory for the mechanisms controlling
611 abundance, diversity, and biogeochemical role of lytic bacterial viruses in
612 aquatic systems. *Limnol. Oceanogr.* **45**, 1320–1328 (2000).
613 14. Knowles, B. *et al.* Lytic to temperate switching of viral communities. *Nature*
614 **531**, 466–470 (2016).
615 15. Suttle, C. a. Marine viruses--major players in the global ecosystem. *Nat. Rev.*
616 *Microbiol.* **5**, 801–12 (2007).

617 16. Fuhrman, J. a. Marine viruses and their biogeochemical and ecological
618 effects. *Nature* **399**, 541–8 (1999).
619 17. Silveira, C. B. *et al.* Viral predation pressure on coral reefs. *BMC Biol.* **21**, 77
620 (2023).
621 18. Friman, V.-P. & Buckling, A. Phages can constrain protist predation-driven
622 attenuation of Pseudomonas aeruginosa virulence in multienemy
623 communities. *ISME J.* **8**, 1820–1830 (2014).
624 19. Aijaz, I. & Koudelka, G. B. Cheating, facilitation and cooperation regulate the
625 effectiveness of phage-encoded exotoxins as antipredator molecules.
626 *Microbiologyopen* **8**, e00636 (2019).
627 20. Brüssow, H. Bacteria between protists and phages: from antipredation
628 strategies to the evolution of pathogenicity. *Mol. Microbiol.* **65**, 583–589
629 (2007).
630 21. Cram, J., Parada, A. & Fuhrman, J. Dilution reveals how viral lysis and grazing
631 shape microbial communities. *Limnol. Oceanogr.* **61**, 889–905 (2016).
632 22. Fuhrman, J. A. & Noble, R. T. Viruses and protists cause similar bacterial
633 mortality in coastal seawater. *Limnol. Oceanogr.* **40**, 1236–1242 (1995).
634 23. Knowles, B. & Rohwer, F. Knowles & Rohwer Reply. *Nature* **549**, E3–E4 (2017).
635 24. Breitbart, M., Bonnain, C., Malki, K. & Sawaya, N. A. Phage puppet masters of
636 the marine microbial realm. *Nat. Microbiol.* **3**, 754–766 (2018).
637 25. Brum, J. R. *et al.* Patterns and ecological drivers of ocean viral communities.
638 *Science* **348**, 1261498 (2015).
639 26. Hurwitz, B. L. & U'Ren, J. M. Viral metabolic reprogramming in marine
640 ecosystems. *Curr. Opin. Microbiol.* **31**, 161–168 (2016).
641 27. Howard-Varona, C. *et al.* Phage-specific metabolic reprogramming of
642 virocells. *ISME J.* **14**, 881–895 (2020).
643 28. Roach, T. N. *et al.* A multiomic analysis of in situ coral–turf algal interactions.
644 *Proc. Natl. Acad. Sci.* **117**, 13588–13595 (2020).
645 29. Thompson, L. R. *et al.* Phage auxiliary metabolic genes and the redirection of
646 cyanobacterial host carbon metabolism. *Proc. Natl. Acad. Sci. U. S. A.* **108**,
647 E757-64 (2011).
648 30. Thompson, L. R., Zeng, Q. & Chisholm, S. W. Gene expression patterns during
649 light and dark infection of Prochlorococcus by cyanophage. *PloS One* **11**,
650 e0165375 (2016).
651 31. Roitman, S. *et al.* Closing the gaps on the viral photosystem-I psa DCAB gene
652 organization. *Environ. Microbiol.* **17**, 5100–5108 (2015).

32. Lehninger, A. L. Bioenergetics. The molecular basis of biological energy transformations. https://www.cabidigitallibrary.org/doi/full/10.5555/19671403907 (1965).
33. Baer, J. *et al.* Viralization as a microbial approach for enhancing coral reef restoration. *ISME J.* **19**, wraf110 (2025).
34. Haas, A. F. *et al.* Unraveling the unseen players in the ocean-a field guide to water chemistry and marine microbiology. *JoVE J. Vis. Exp.* e52131 (2014).
35. Sambrook, J., Fritsch, E. F. & Maniatis, T. *Molecular Cloning: A Laboratory Manual.* (1989).
36. Thurber, R. V., Haynes, M., Breitbart, M., Wegley, L. & Rohwer, F. Laboratory procedures to generate viral metagenomes. *Nat. Protoc.* **4**, 470–483 (2009).
37. Lücking, D., Mercier, C., Alarcón-Schumacher, T. & Erdmann, S. Extracellular vesicles are the main contributor to the non-viral protected extracellular sequence space. *ISME Commun.* **3**, 112 (2023).
38. Schmieder, R. & Edwards, R. Quality control and preprocessing of metagenomic datasets. *Bioinformatics* **27**, 863–864 (2011).
39. Schmieder, R., Lim, Y. W., Rohwer, F. & Edwards, R. TagCleaner: Identification and removal of tag sequences from genomic and metagenomic datasets. *BMC Bioinformatics* **11**, 1–14 (2010).
40. Schmieder, R. & Edwards, R. Fast identification and removal of sequence contamination from genomic and metagenomic datasets. *PloS One* **6**, e17288 (2011).
41. Meyer, F. *et al.* The metagenomics RAST server – a public resource for the automatic phylogenetic and functional analysis of metagenomes. *BMC Bioinformatics* **9**, 386 (2008).
42. Kelly, L. W. *et al.* Black reefs: iron-induced phase shifts on coral reefs. *ISME J.* **6**, 1–12 (2011).
43. Barott, K. L. *et al.* Microbial to reef scale interactions between the reef-building coral Montastraea annularis and benthic algae. *Proc. R. Soc. B Biol. Sci.* **279**, 1655–1664 (2012).
44. George, E. E. *et al.* Space-filling and benthic competition on coral reefs. *PeerJ* **9**, e11213 (2021).
45. Barott, K. *et al.* Hyperspectral and physiological analyses of coral-algal interactions. *PloS One* **4**, e8043 (2009).
46. Pirovich, D. B., Da'dara, A. A. & Skelly, P. J. Multifunctional fructose 1, 6-bisphosphate aldolase as a therapeutic target. *Front. Mol. Biosci.* **8**, 719678 (2021).

690 47. Webb, E. C. *Enzyme Nomenclature 1992. Recommendations of the*
691 *Nomenclature Committee of the International Union of Biochemistry and*
692 *Molecular Biology on the Nomenclature and Classification of Enzymes.*
693 (Academic Press, 1992).
694 48. Srinivasan, P., Katagiri, M. & Sprinson, D. B. The conversion of
695 phosphoenolpyruvic acid and d-erythrose 4-phosphate to 5-dehydroquinic
696 acid. *J. Biol. Chem.* **234**, 713–715 (1959).
697 49. Knowles, B. *et al.* Variability and host density independence in inductions-
698 based estimates of environmental lysogeny. *Nat. Microbiol.* **2**, 17064 (2017).
699 50. Knowles, B. *et al.* Temperate infection in a virus–host system previously known
700 for virulent dynamics. *Nat. Commun.* **11**, 1–13 (2020).
701 51. Howard-Varona, C., Hargreaves, K. R., Abedon, S. T. & Sullivan, M. B.
702 Lysogeny in nature: mechanisms, impact and ecology of temperate phages.
703 *ISME J.* **11**, 1511 (2017).
704 52. Hurwitz, B. L., Hallam, S. J. & Sullivan, M. B. Metabolic reprogramming by
705 viruses in the sunlit and dark ocean. *Genome Biol.* **14**, 1–14 (2013).
706 53. Devoto, A. E. *et al.* A new family of "megaphages" abundant in the marine
707 environment. *Nat. Microbiol.* **6**, 123–131 (2021).
708 54. Anantharaman, K. *et al.* Sulfur oxidation genes in diverse deep-sea viruses.
709 *Science* **344**, 757–760 (2014).
710 55. Moniruzzaman, M., Martinez-Gutierrez, C. A., Weinheimer, A. R. & Aylward, F.
711 O. Dynamic genome evolution and complex virocell metabolism of globally-
712 distributed giant viruses. *Nat. Commun.* **11**, 1710 (2020).
713 56. Ha, A. D., Moniruzzaman, M. & Aylward, F. O. High transcriptional activity and
714 diverse functional repertoires of hundreds of giant viruses in a coastal marine
715 system. *mSystems* **6**, e0074321 (2021).
716 57. Rodrigues, R. A. L., Arantes, T. S., Oliveira, G. P., Silva, L. K. & Abrahão, J. S. The
717 complex nature of Tupanviruses. *Adv. Virus Res.* **103**, 135–162 (2019).
718 58. Schroeder, D. C. & others. Viruses infecting a warm water picoeukaryote
719 shed light on spatial and temporal patterns in virus community ecology. *ISME*
720 *J.* **15**, 3621–3634 (2021).
721

722 **Tables and Figures.**

723 **Table 1: Central Carbon Metabolism genes shown in Figures 2 and 3.** Genes are categorized
724 by pathway and gene function, identified by EC number and gene name, and annotated
725 with prior references if they have been observed in viruses before. The Spearman's
726 correlation between the frequency of each gene and viromes temperateness is indicated
727 by bootstrapped mean ρ_s values and 95 % confidence intervals from 1,000 iterations are
728 shown. Please refer to **Supplementary Figure 2** for bootstrap ρ_s distributions. Genes where
729 the 95 % confidence intervals exclude zero are significant at the $p < 0.05$ level. Genes shared
730 between pathways are shown with a slash. Note, although anaplerotic and cataplerotic
731 reactions often refer to steps in the TCA, we are using the term more generally here to refer
732 respectively to the generation of central intermediate metabolites ('filling up'; anaplerotic) and
733 the consumption of central metabolites to generate specialized pre-cursor or cellular energy
734 pools ('drawing down'; cataplerotic) more generally[32]. Bootstrapping code can be found at
735 https://github.com/hopefulmonstersucla/viral-metabolism/tree/main/code.

EC number	SEED database gene name	Pathway	Gene activity	ρ_s	95 % CI	Observed in viruses
1.1.1.37	Malate dehydrogenase	Tricarboxylic Acid	Cataplerotic	-0.19	-0.61, 0.29	
1.1.1.41	Isocitrate dehydrogenase [NAD]	Tricarboxylic Acid	Cataplerotic	-0.13	-0.54, 0.34	
1.1.1.42	Isocitrate dehydrogenase [NADP]	Tricarboxylic Acid	Cataplerotic	-0.19	-0.63, 0.29	[52,53]
1.1.1.44	6-phosphogluconate dehydrogenase	Pentose Phosphate	Anaplerotic	-0.06	-0.54, 0.45	[29,52,54]
1.1.1.49	Glucose-6-phosphate 1-dehydrogenase	ED glycolysis/ Pentose Phosphate	Anaplerotic	0.26	-0.24, 0.68	
1.2.1.12	NAD-dependent glyceraldehyde-3-phosphate dehydrogenase	EMP glycolysis/ Gluconeogenesis	Cataplerotic	-0.20	-0.60, 0.26	
1.2.4.1	Pyruvate dehydrogenase	Tricarboxylic Acid	Cataplerotic	-0.12	-0.60, 0.36	[52]
1.2.4.2	2-oxoglutarate dehydrogenase	Tricarboxylic Acid	Cataplerotic	-0.10	-0.59, 0.42	
2.2.1.1	Transketolase	Pentose Phosphate		-0.08	-0.52, 0.35	[29,52,54]
2.2.1.2	Transaldolase	Pentose Phosphate	Cataplerotic	-0.49	-0.87, 0.02	[7,45,47]
2.3.3.1	Citrate synthase	Tricarboxylic Acid		0.15	-0.32, 0.56	
2.3.3.9	Malate synthase	Tricarboxylic Acid	Anaplerotic	0.61	0.20, 0.90*	[55]
2.7.1.11	6-phosphofructokinase	EMP glycolysis	Cataplerotic	-0.03	-0.48, 0.45	
2.7.1.40	Pyruvate kinase	EMP glycolysis	Cataplerotic	0.42	0.04, 0.74*	
2.7.2.3	Phosphoglycerate kinase	EMP glycolysis/ Gluconeogenesis	Cataplerotic	0.03	-0.41, 0.47	
3.1.1.31	6-phosphogluconolactonase	ED glycolysis/ Pentose Phosphate	Anaplerotic	0.43	0.03, 0.77*	
3.1.3.11	Fructose-1,6-bisphosphatase	Gluconeogenesis	Anaplerotic	0.24	-0.20, 0.66	[55]
4.1.1.31	Phosphoenolpyruvate carboxylase	Gluconeogenesis	Anaplerotic	0.45	0.00, 0.77*	
4.1.1.32	Phosphoenolpyruvate carboxykinase [GTP]	Gluconeogenesis		0.11	-0.39, 0.57	[55,56]
4.1.2.13 I	Fructose-bisphosphate aldolase class I	EMP glycolysis/ Gluconeogenesis	Cataplerotic	-0.65	-0.86, 0.33	
4.1.2.13 II	Fructose-bisphosphate aldolase class II	EMP glycolysis/ Gluconeogenesis	Cataplerotic	0.56	-0.18, 0.83	
4.1.2.14	2-dehydro-3-deoxyphosphogluconate aldolase	ED glycolysis	Anaplerotic	0.67	0.36, 0.90*	

4.1.3.1	Isocitrate lyase	Tricarboxylic Acid		-0.10	-0.54, 0.37	
4.2.1.11	Enolase	EMP glycolysis/ Gluconeogenesis		0.43	0.02, 0.76*	[55]
4.2.1.12	Phosphogluconate dehydratase	ED glycolysis	Anaplerotic	0.71	0.47, 0.89*	
4.2.1.2	Fumarate hydratase class II	Tricarboxylic Acid		0.29	-0.15, 0.68	
4.2.1.3	Aconitate hydratase	Tricarboxylic Acid		-0.35	-0.71, 0.13	[55,57]
5.1.3.1	Ribulose-phosphate 3-epimerase	Pentose Phosphate		0.03	-0.45, 0.49	[58]
5.3.1.1	Triosephosphate isomerase	EMP glycolysis/ Gluconeogenesis		-0.02	-0.44, 0.41	[55]
5.3.1.6	Ribose 5-phosphate isomerase	Pentose Phosphate		0.32	-0.14, 0.68	[54]
5.3.1.9	Glucose-6-phosphate isomerase	EMP glycolysis/ Gluconeogenesis		0.45	0.12, 0.73*	
5.4.2.11	Phosphoglycerate mutase	EMP glycolysis/ Gluconeogenesis		-0.46	-0.80, 0.01	[55,56]
5.4.2.12	2,3-bisphosphoglycerate-independent phosphoglycerate mutase	EMP glycolysis/ Gluconeogenesis		0.41	-0.01, 0.73	
6.2.1.5a	Succinyl-CoA ligase [ADP-forming] alpha chain	Tricarboxylic Acid		0.17	-0.33, 0.61	
6.2.1.5b	Succinyl-CoA ligase [ADP-forming] beta chain	Tricarboxylic Acid		-0.04	-0.52, 0.41	

736

737

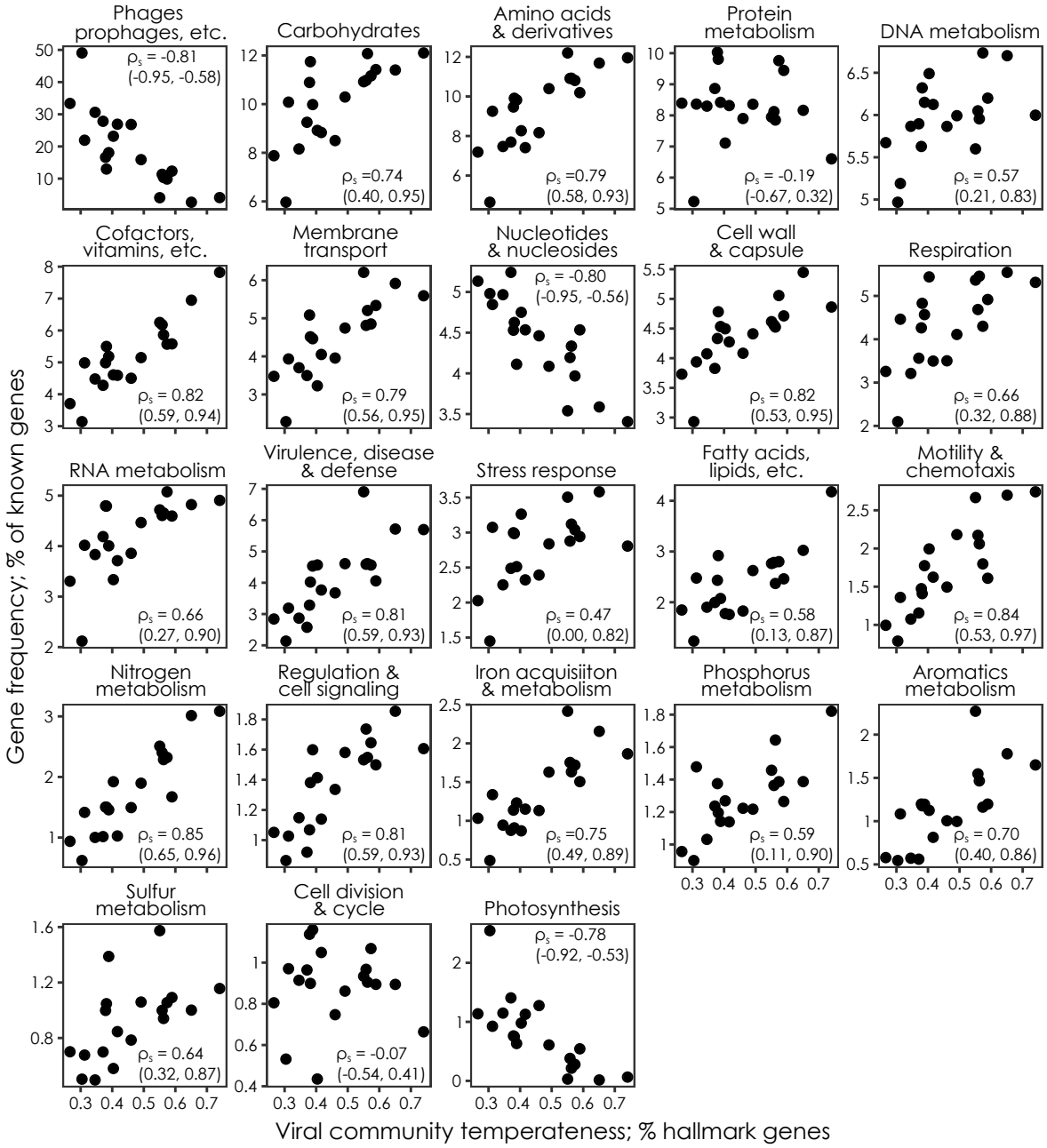

Figure 1: Correlations between metabolic function and community temperateness across the breadth of cellular metabolism. Spearman's rho estimates (ρ_s) are shown with 95 % confidence intervals (CIs) in parentheses from 1,000 bootstrapped simulations. Panels are ordered by mean gene frequency. The y-axis shows the gene frequency as a percentage of known genes, an internally normalized and relative metric where all of the frequencies for a given sample across all panels sums to 100 %. Gene categories with average frequencies below 0.5 % were omitted. Viral community temperateness was calculated as the percentage of integrase and excision genes in the known genes in each virome. Genes where the 95 % confidence intervals exclude zero are significant at the $p < 0.05$ level. Bootstrapping code can be found at https://github.com/hopefulmonstersucla/viral-metabolism/tree/main/code.

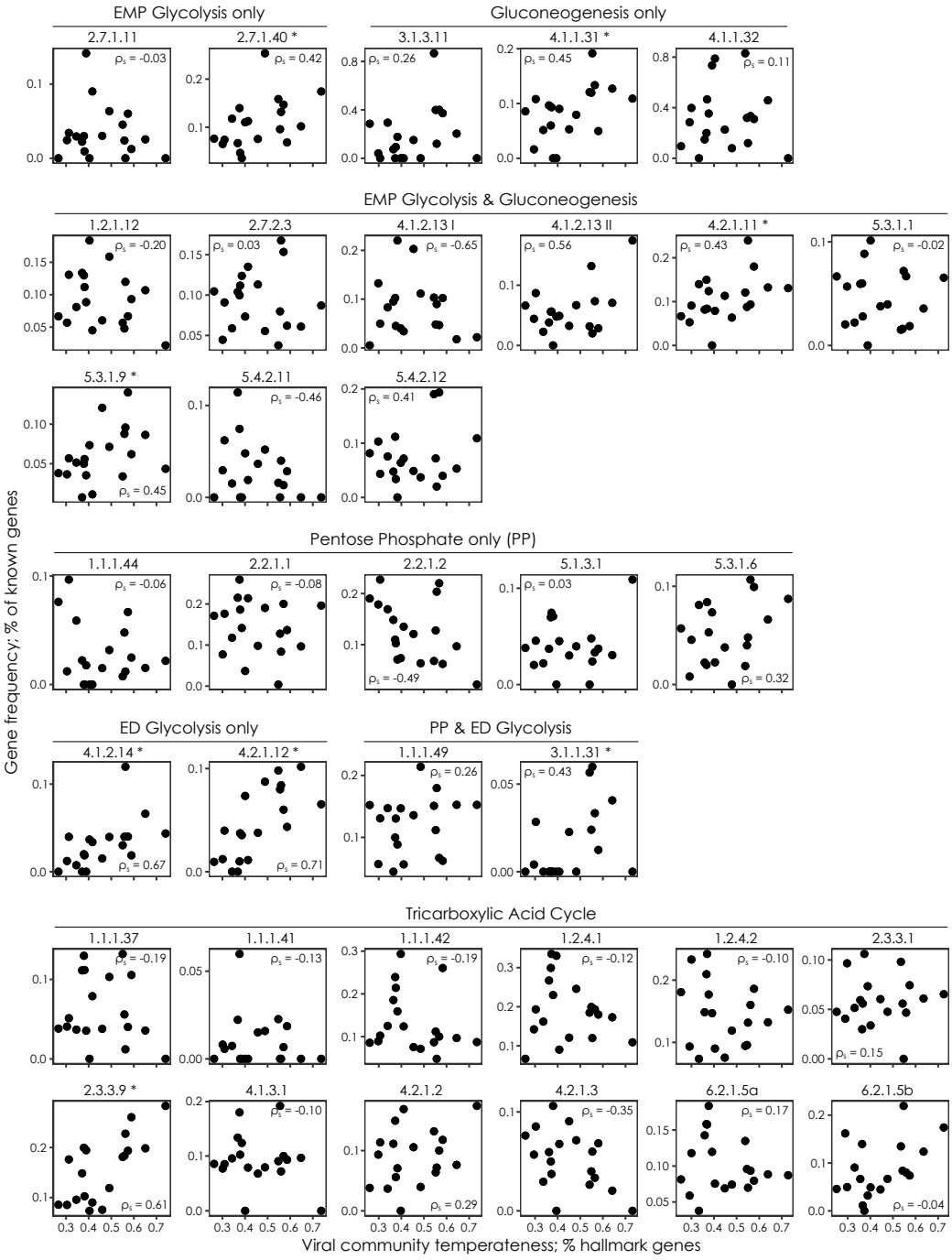

Figure 2: Correlation between central carbon metabolism genes and viral community temperateness. Spearman's rho correlation coefficients (ρ_s) are shown from 1,000 bootstrapped simulations correlating central carbon metabolism gene frequency as a percentage of known genes vs viral community temperateness. Panels are ordered by pathway, including Embden-Meyerhof-Parnas glycolysis (EMP), Entner-Doudoroff glycolysis (ED), pentose phosphate (PP), and tricarboxylic acid cycle pathways. Viral community temperateness was calculated as the percentage of integrase and excision genes in the known genes in each virome. Enzymes with rho values significantly different to zero are indicated by asterisks (i.e., $p < 0.05$, 95 % confidence intervals exclude zero). Genes are labeled by EC numbers; see **Table 1** for gene names and summary statistics.

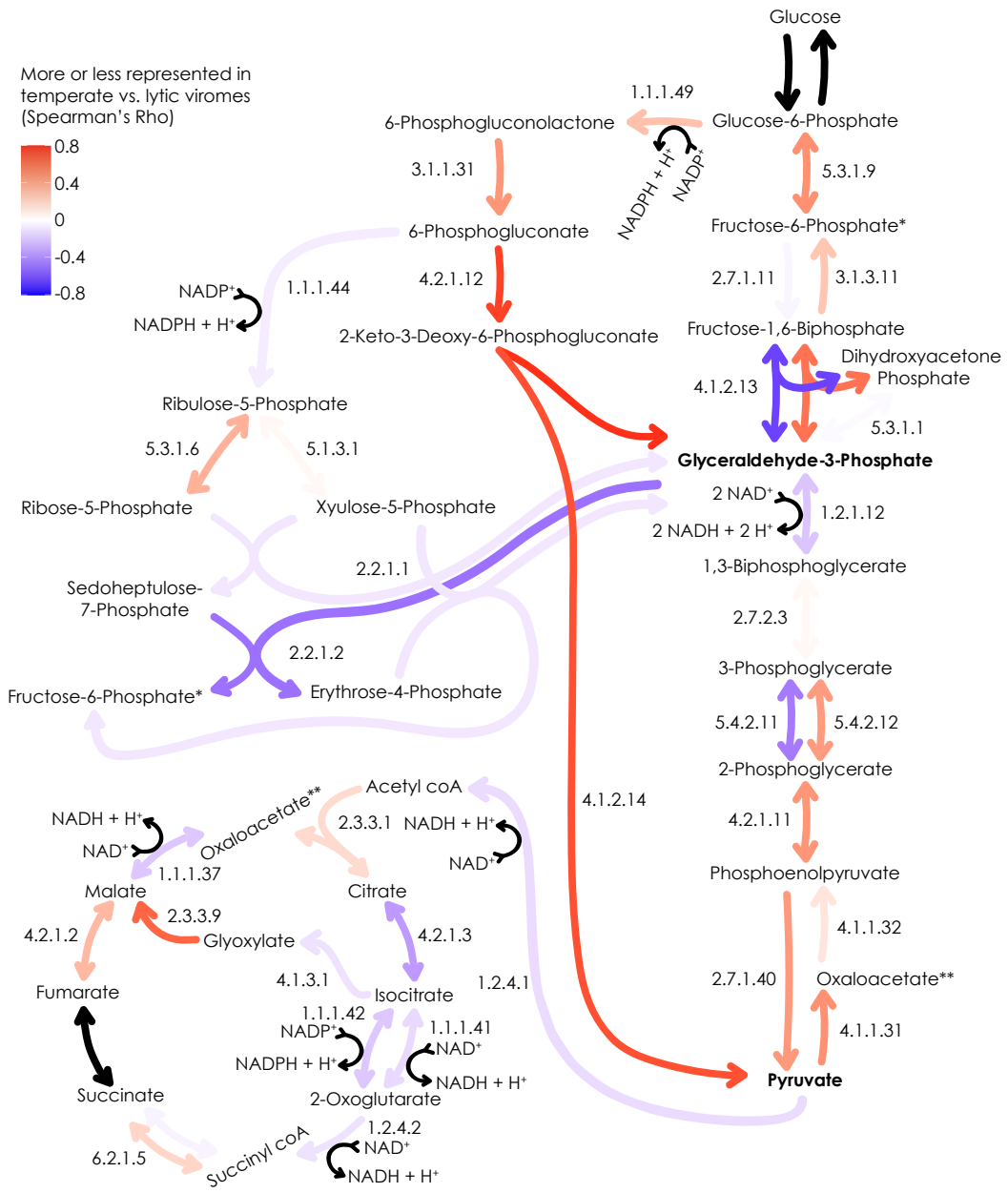

Figure 3: Pathway map of changes in the frequency of central carbon metabolism genes across the lytic to temperate spectrum. Map of central carbon metabolism with each enzymatic step colored by the change in enzymatic metagenomic gene frequency across lytic to temperate viral communities. Red arrows show higher frequency in temperate communities while blue arrows are lytic associated, reflecting ρ_s values for each enzyme as seen in **Table 1** and **Figure 2**. Enzymes are labeled by EC numbers (see **Table 1** for gene names). Single-headed and double-headed arrows represent irreversible and reversible reactions, respectively. Black arrows show genes that were absent from all viromes. Central intermediate metabolites glyceraldehyde-3-phosphate (G3P) and pyryvate are shown in bold. *Note that fructose-6-phosphate is found in the EMP/gluconeogenesis pathways as well as the PPP, ** that oxaloacetate is produced in both the TCA and gluconeogenesis, and that EC1.1.1.42 in the TCA has an oxalosuccinate intermediate. Code can be found at https://github.com/hopefulmonstersucla/viral-metabolism/tree/main/code.

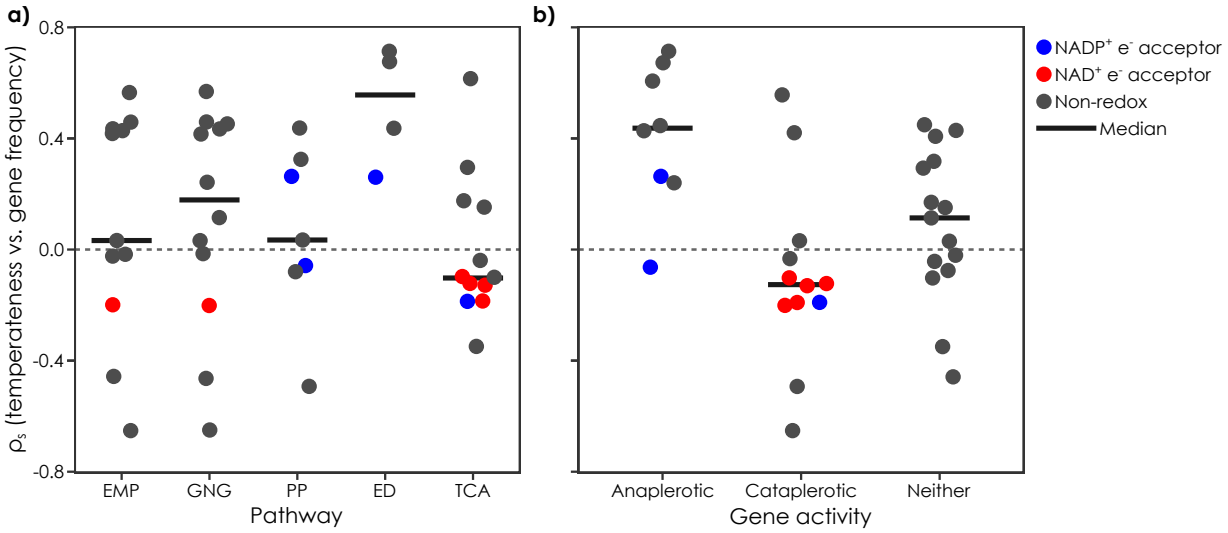

774
775 **Figure 4: Correlations between viral community temperateness and central carbon gene**
776 **frequency across pathways and gene function. (a)** Spearman's rho correlation coefficients (ρ_s)
777 for genes in the Embden- Meyerhof-Parnas glycolysis (EMP), gluconeogenesis (GNG), pentose
778 phosphate (PP), Entner-Doudoroff glycolysis (ED, and tricarboxylic acid cycle (TCA) pathways
779 are shown with median values marked by horizontal bars in each pathway. (b) Coefficients are
780 also shown for genes involved in building up central intermediate metabolite pools like pyruvate
781 and glyceraldehyde-3-phosphate (anaplerotic reactions) or consuming general metabolites to
782 make specialized pools of precursors and cellular energy (cataplerotic reactions) in central
783 carbon metabolism, compared with genes involved in neither anaplerosis nor cataplerosis, also
784 with median values shown. Oxidoreductase genes are colored by their electron acceptor: blue
785 for $NADP^+$ electron acceptors involved in biomass generation, and red for NAD^+ electron
786 acceptors involved in cellular energy generation. Dashed horizontal lines indicate $\rho_s = 0$. Note,
787 although anaplerotic and cataplerotic reactions often refer to steps in the TCA, we are using the
788 term more generally here to refer respectively to the generation ('filling up'; anaplerotic) of
789 flexible general intermediate metabolites and the consumption of general metabolites towards
790 precursor and cellular energy production ('drawing down'; cataplerotic) more generally[32].
791

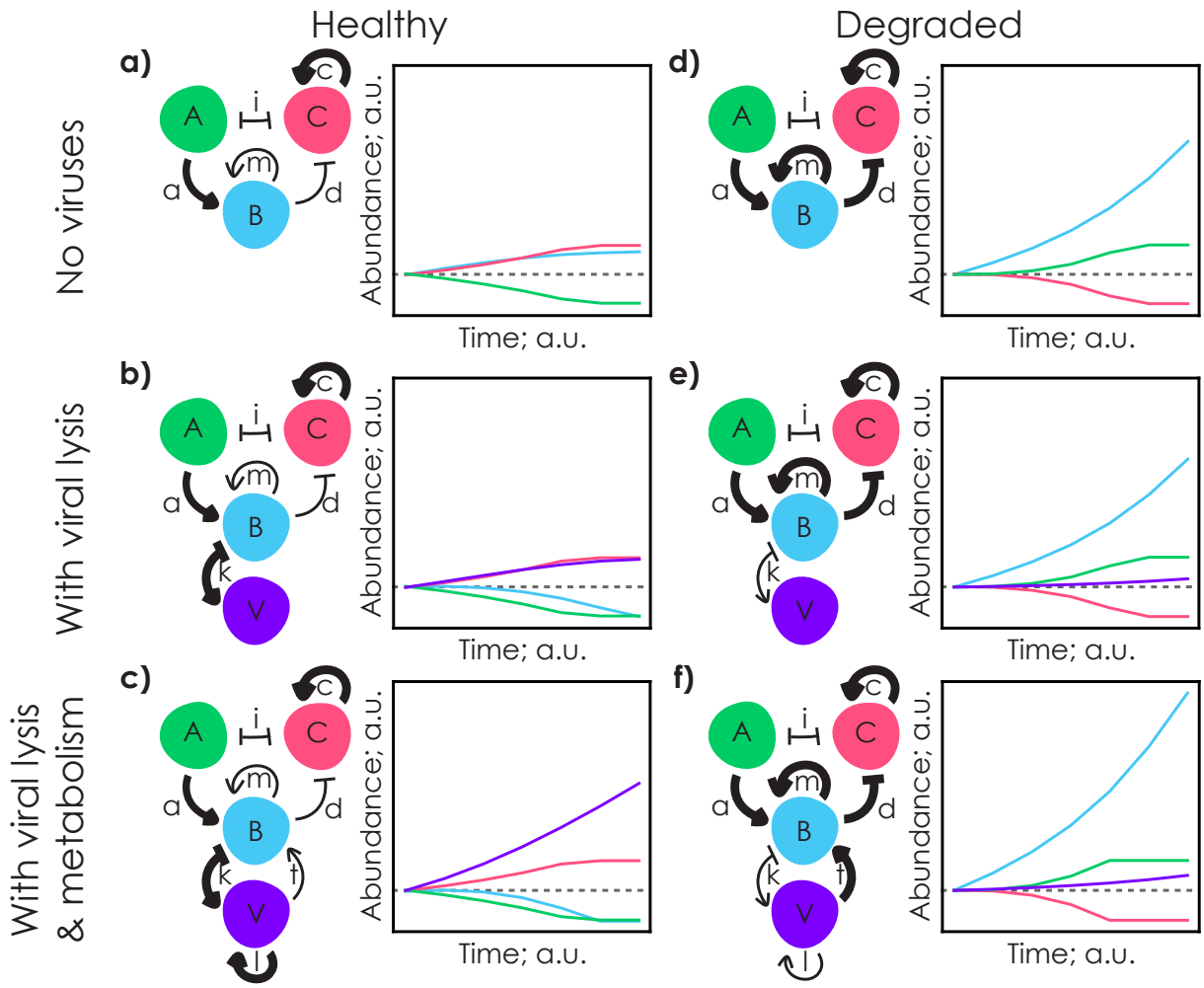

Figure 5: Schematic model incorporating viral metabolic effects on resilience of healthy coral reefs and exacerbation of reef degradation. The predicted effects of viral lysis and metabolic capability on algal (A; green), coral (C; coral), bacteria (B; blue) and viral (V; violet) population sizes in healthy and degraded reef scenarios with no viruses (a and d, respectively), with viral lysis (b and e, respectively), and with viral lysis and metabolism (c and f, respectively). Compartment models showing how the model was implemented for each panel are shown (left) as well as resulting dynamics (right). Dynamics show changes in populations over time, in arbitrary units (a.u.), reflecting the qualitative nature of the model. In each iteration, algal population size A was solved as the 1 – C to reflect the finite space available on the benthos. Parameter values, shown as line weights, qualitatively reflect known processes on healthy vs degraded reefs, and can be found in **Supplementary Table 2**. Rates include: (i) coral-algal inhibition, (c) coral proliferation, (a) algal-mediated DOC supply to bacteria, (m) bacterial anabolic metabolism, (d) bacterial-mediate coral disease, (k) viral lysis of bacteria, (l) lytic viral metabolism, and (t) temperate viral metabolism. Note that panels **(b)** and **(e)** depict the Kill-the-Winner and Piggyback-the-Winner models, respectively. Algal, coral, bacteria, and viral pools were initialized at 0.5 a.u. for all simulations where present. To make the model as conservative as possible, rates of algal carbon delivery (a), and direct coral-algal interference (i) were not changed across scenarios; doing so would lead to enhanced loss of coral. Note that flat lines at minimal values reflect functional population extinction.

813 **Legends only**

814 **Table 1: Central Carbon Metabolism genes shown in Figures 2 and 3.** Genes are
815 categorized by pathway and gene function, identified by EC number and gene
816 name, and annotated with prior references if they have been observed in
817 viruses before. The Spearman's correlation between the frequency of each
818 gene and viromes temperateness is indicated by bootstrapped mean ρ_s values
819 and 95 % confidence intervals from 1,000 iterations are shown. Please refer to
820 **Supplementary Figure 2** for bootstrap ρ_s distributions. Genes where the 95 %
821 confidence intervals exclude zero are significant at the $p < 0.05$ level. Genes
822 shared between pathways are shown with a slash. Note, although anaplerotic
823 and cataplerotic reactions often refer to steps in the TCA, we are using the term
824 more generally here to refer respectively to the generation of central
825 intermediate metabolites ('filling up'; anaplerotic) and the consumption of
826 central metabolites to generate specialized pre-cursor or cellular energy pools
827 ('drawing down'; cataplerotic) more generally[32]. Bootstrapping code can be
828 found at https://github.com/hopefulmonstersucla/viral-
829 metabolism/tree/main/code.

830 **Figure 1: Correlations between metabolic function and community**
831 **temperateness across the breadth of cellular metabolism.** Spearman's rho
832 estimates (ρ_s) are shown with 95 % confidence intervals (CIs) in parentheses from
833 1,000 bootstrapped simulations. Panels are ordered by mean gene frequency.
834 The y-axis shows the gene frequency as a percentage of known genes, an
835 internally normalized and relative metric where all of the frequencies for a given
836 sample across all panels sums to 100 %. Gene categories with average
837 frequencies below 0.5 % were omitted. Viral community temperateness was
838 calculated as the percentage of integrase and excision genes in the known
839 genes in each virome. Genes where the 95 % confidence intervals exclude zero
840 are significant at the $p < 0.05$ level. Bootstrapping code can be found at
841 https://github.com/hopefulmonstersucla/viral-metabolism/tree/main/code.

842 **Figure 2: Correlation between central carbon metabolism genes and viral**
843 **community temperateness.** Spearman's rho estimates (ρ_s) are shown from 1,000
844 bootstrapped simulations correlating central carbon metabolism gene
845 frequency as a percentage of known genes vs viral community temperateness.
846 Panels are ordered by pathway, including Embden- Meyerhof-Parnas glycolysis
847 (EMP), Entner-Doudoroff glycolysis (ED), pentose phosphate (PP), and
848 tricarboxylic acid cycle pathways. Viral community temperateness was
849 calculated as the percentage of integrase and excision genes in the known
850 genes in each virome. Enzymes with rho values significantly different to zero are
851 indicated by asterisks (i.e., $p< 0.05$, 95 % confidence intervals exclude zero).
852 Genes are labeled by EC numbers; see **Table 1** for gene names and summary
853 statistics.

854 **Figure 3: Figure 3: Pathway map of changes in the frequency of central carbon**
855 **metabolism genes across the lytic to temperate spectrum.** Map of central
856 carbon metabolism with each enzymatic step colored by the change in
857 enzymatic metagenomic gene frequency across lytic to temperate viral
858 communities. Enzymes are labeled by EC numbers (see **Table 1** for gene names).
859 Red arrows show higher frequency in temperate communities while blue arrows
860 are lytic associated, reflecting ρ_s values for each enzyme as seen in **Table 1** and
861 **Figure 2**. Single-headed and double-headed arrows represent irreversible and
862 reversible reactions, respectively. Black arrows show genes that were absent
863 from all viromes. Central intermediate metabolites glyceraldehyde-3-phosphate
864 (G3P) and pyryvate are shown in bold. *Note that fructose-6-phosphate is found
865 in the EMP/gluconeogenesis pathways as well as the PPP, ** that oxaloacetate is
866 produced in both the TCA and gluconeogenesis, and that EC1.1.1.42 in the TCA
867 has an intermediate oxalosuccinate product/substrate. Code can be found at
868 https://github.com/hopefulmonstersucla/viral-metabolism/tree/main/code.

869 **Figure 4: Correlations between viral community temperateness and central**
870 **carbon gene frequency across pathways and gene function. (a)** Spearman's
871 rho correlation coefficients (ρ_s) for genes in the Embden- Meyerhof-Parnas
872 glycolysis (EMP), gluconeogenesis (GNG), pentose phosphate (PP), Entner-
873 Doudoroff glycolysis (ED, and tricarboxylic acid cycle (TCA) pathways are shown
874 with median values marked by horizontal bars in each pathway. (b) Coefficients
875 are also shown for genes involved in building up central intermediate
876 metabolite pools like pyruvate and glyceraldehyde-3-phosphate (anaplerotic
877 reactions) or consuming general metabolites to make specialized pools of
878 precursors and cellular energy (cataplerotic reactions) in central carbon
879 metabolism, compared with genes involved in neither anaplerosis nor
880 cataplerosis, also with median values shown. Oxidoreductase genes are colored
881 by their electron acceptor: blue for $NADP^+$ electron acceptors involved in
882 biomass generation, and red for NAD^+ electron acceptors involved in cellular
883 energy generation. Dashed horizontal lines indicate $\rho_s = 0$. Note, although
884 anaplerotic and cataplerotic reactions often refer to steps in the TCA, we are
885 using the term more generally here to refer respectively to the generation ('filling
886 up'; anaplerotic) of flexible general intermediate metabolites and the
887 consumption of general metabolites towards precursor and cellular energy
888 production ('drawing down'; cataplerotic) more generally.

889 **Figure 5: Schematic model incorporating viral metabolic effects on resilience of**
890 **healthy coral reefs and exacerbation of reef degradation.** The predicted effects
891 of viral lysis and metabolic capability on algal (A; green), coral (C; coral),
892 bacteria (B; blue) and viral (V; violet) population sizes in healthy and degraded
893 reef scenarios with no viruses (a and d, respectively), with viral lysis (b and e,
894 respectively), and with viral lysis and metabolism (c and f, respectively).
895 Compartment models showing how the model was implemented for each
896 panel are shown (left) as well as resulting dynamics (right). Dynamics show
897 changes in populations over time, in arbitrary units (a.u.), reflecting the

898 qualitative nature of the model. In each iteration, algal population size A was
899 solved as the 1 – C to reflect the finite space available on the benthos.
900 Parameter values, shown as line weights, qualitatively reflect known processes
901 on healthy vs degraded reefs, and can be found in **Supplementary Table 2**.
902 Rates include: (i) coral-algal inhibition, (c) coral proliferation, (a) algal-mediated
903 DOC supply to bacteria, (m) bacterial anabolic metabolism, (d) bacterial-
904 mediate coral disease, (k) viral lysis of bacteria, (l) lytic viral metabolism, and (t)
905 temperate viral metabolism. Note that panels **(b)** and **(e)** depict the Kill-the-
906 Winner and Piggyback-the-Winner models, respectively. Algal, coral, bacteria,
907 and viral pools were initialized at 0.5 for all simulations where present. To make
908 the model as conservative as possible, rates of algal carbon delivery (a), and
909 direct coral-algal interference (i) were not changed across scenarios; doing so
910 would lead to enhanced loss of coral. Note that flat lines at minimal values
911 reflect functional population extinction. Code can be found at
912 https://github.com/hopefulmonstersucla/viral-metabolism/tree/main/code.

913

Figures only

Figure 1

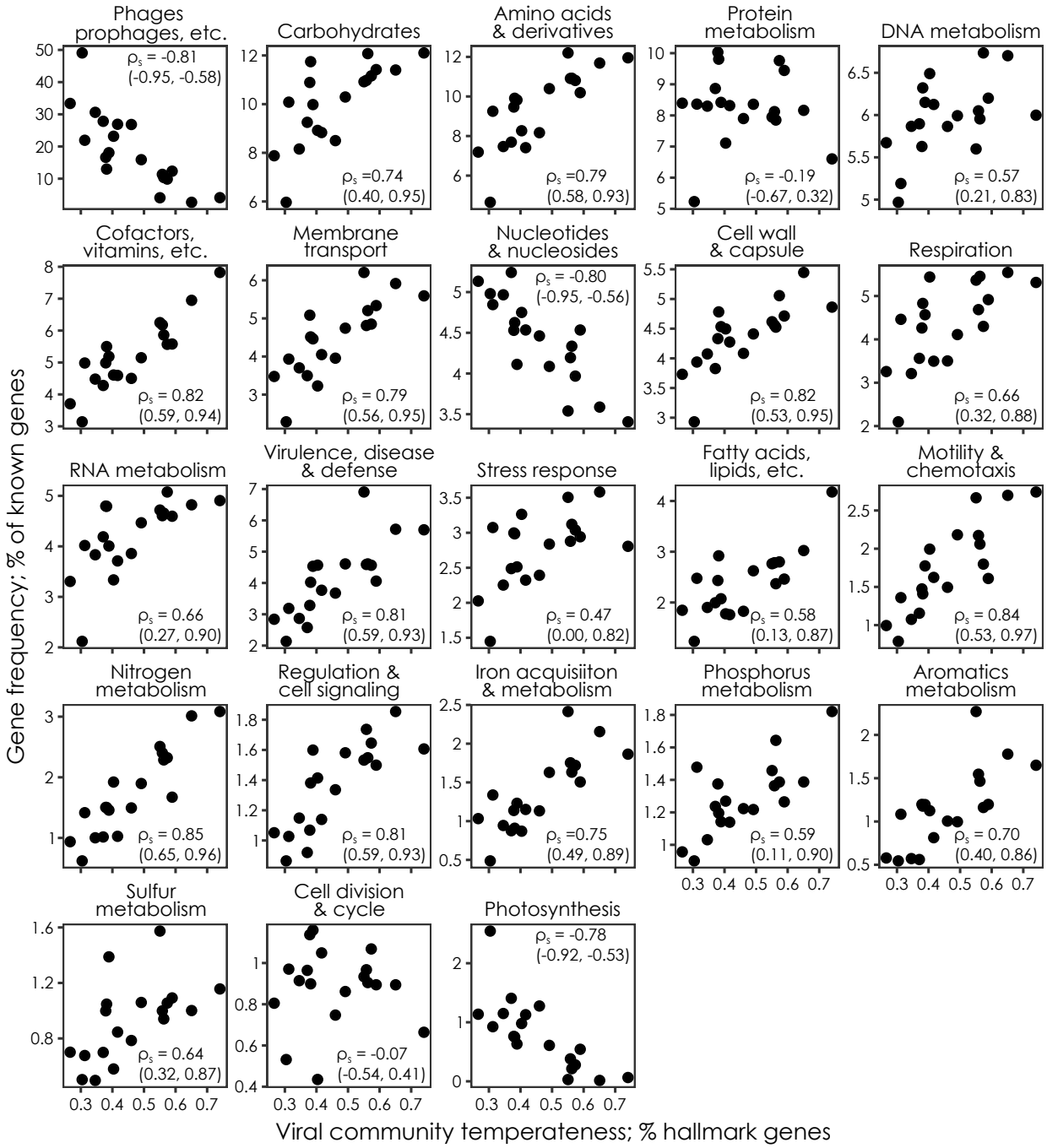

Figure 2

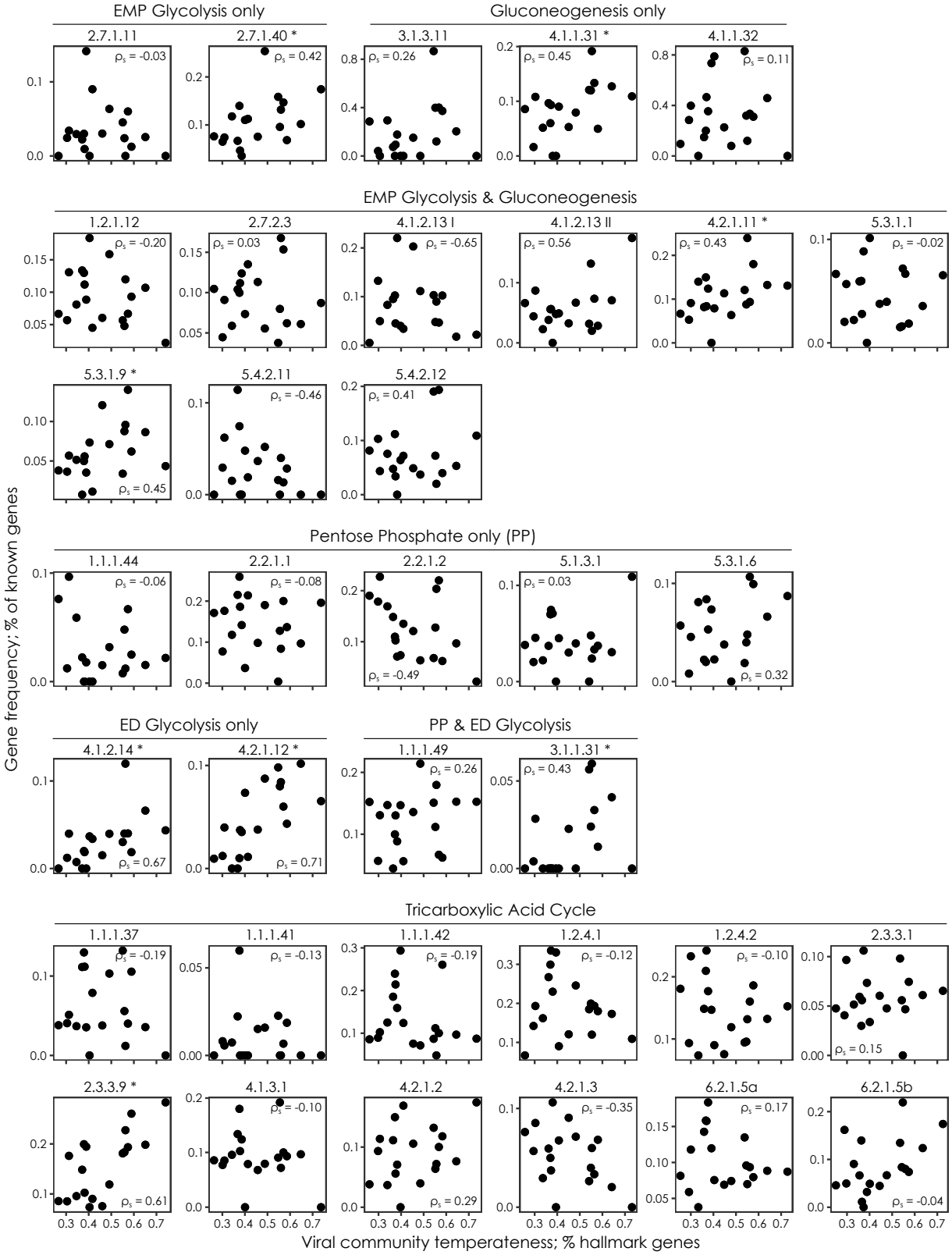
EMP Glycolysis only
Gluconeogenesis only
2.7.1.11
2.7.1.40 *
3.1.3.11
4.1.1.31 *
4.1.1.32
EMP Glycolysis & Gluconeogenesis
1.2.1.12
2.7.2.3
4.1.2.13 I
4.1.2.13 II
4.2.1.11 *
5.3.1.1
5.3.1.9 *
5.4.2.11
5.4.2.12
Pentose Phosphate only (PP)
1.1.1.44
2.2.1.1
2.2.1.2
5.1.3.1
5.3.1.6
ED Glycolysis only
PP & ED Glycolysis
4.1.2.14 *
4.2.1.12 *
1.1.1.49
3.1.1.31 *
Tricarboxylic Acid Cycle
1.1.1.37
1.1.1.41
1.1.1.42
1.2.4.1
1.2.4.2
2.3.3.1
2.3.3.9 *
4.1.3.1
4.2.1.2
4.2.1.3
6.2.1.5a
6.2.1.5b
Gene frequency; % of known genes
Viral community temperateness; % hallmark genes

919 **Figure 3**

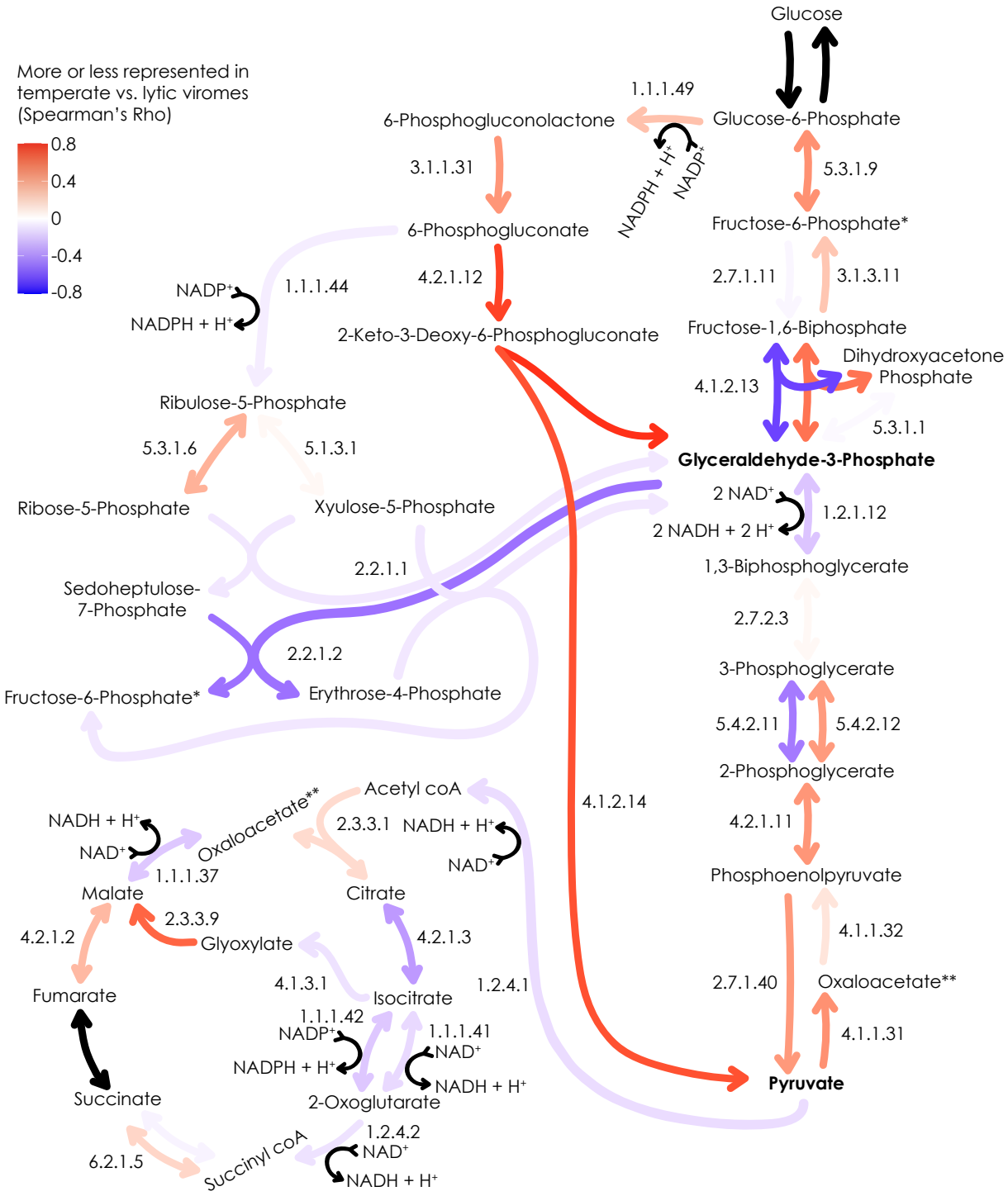

920

921 **Figure 4**

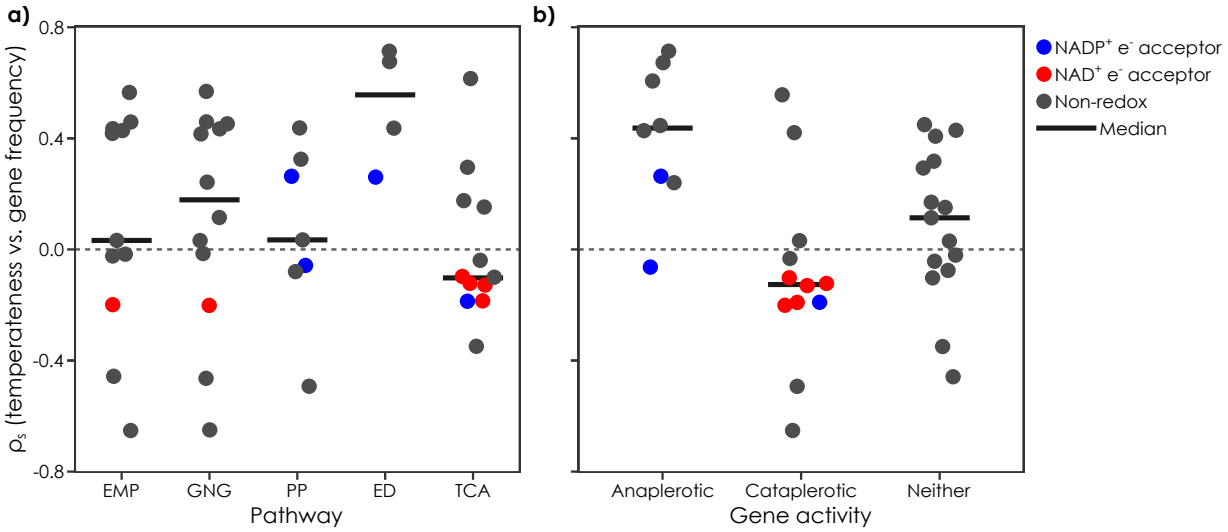

922

923

924

Figure 5

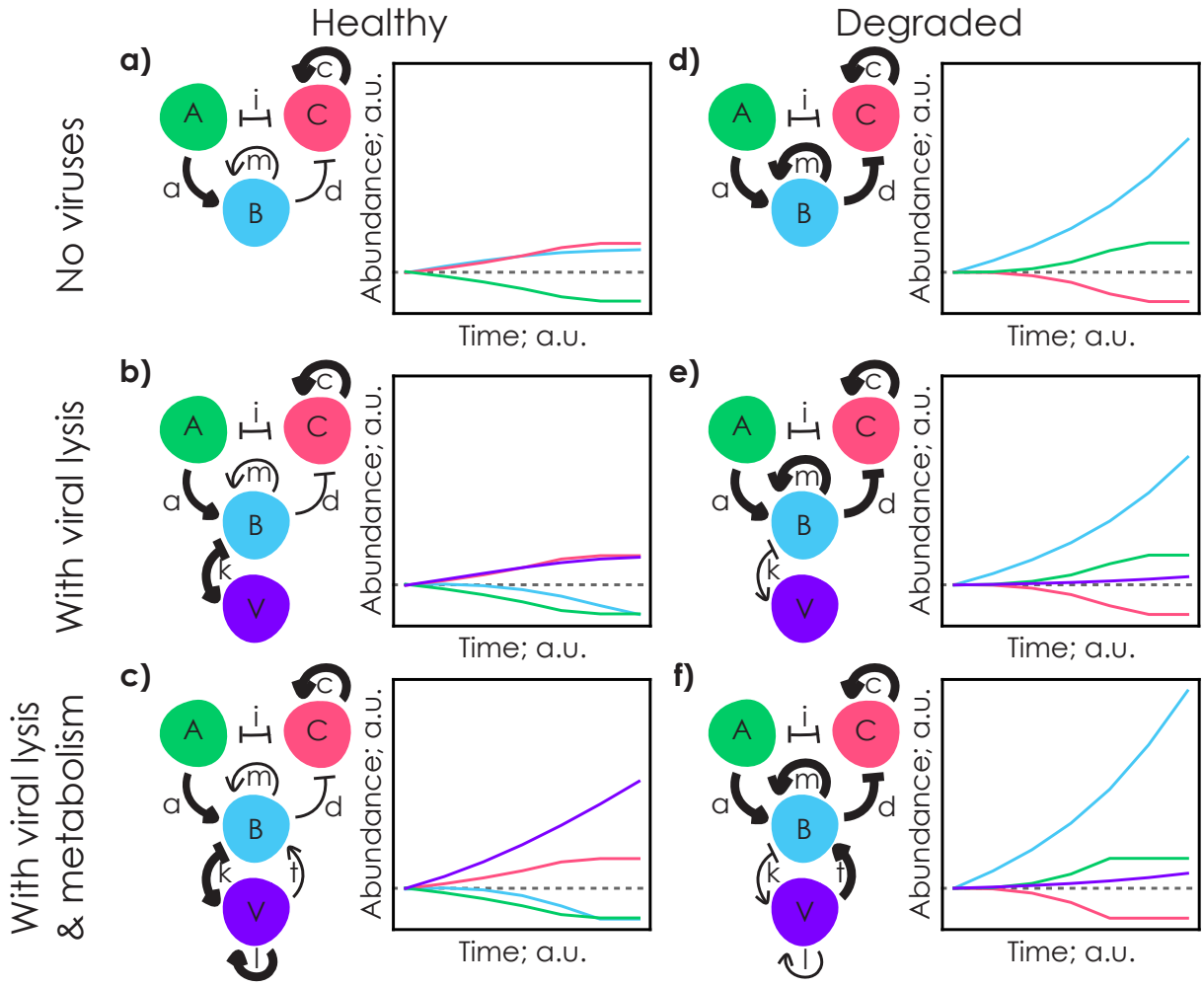
Healthy
Degraded
No viruses
With viral lysis
With viral lysis & metabolism
a)
b)
c)
d)
e)
f)
A
B
C
V
a
c
d
i
k
l
m
†
Abundance; a.u.
Time; a.u.

928 **Supplementary Tables and Figures**

929 **Supplementary Table 1: Summary of the 19 samples analyzed, including sample**
930 **accession numbers, the total number of base pairs, reads sequenced, and**
931 **locations of viral metagenomes.** Note that all metagenomes have been
932 previously published except Pearl and Hermes Reef Wreck and Caroline Wreck
933 Site samples indicated by an asterisk. Caroline Island is now named Millenium
934 Atoll. Fasta files for all metagenomes can be found at
935 https://github.com/hopefulmonstersucla/viral-metabolism/tree/main/fastas.

Sample Location	MG-RAST Accession Number	bp count	Sequence count	Latitude	Longitude
Millennium Atoll	4683670.3	47624434	173813	-9.9138	-150.2038
Flint Atoll	4683674.3	7294624	26673	-11.43	-151.8192
Starbuck	4683677.3	28130343	102666	-5.6384	-155.8811
Maui	4683680.3	48918703	178536	20.86447	-156.13911
Oahu	4683683.3	28708747	104972	21.4389	-158
Pearl & Hermes Reef	4683684.3	211441921	771690	27.8557	-175.8318
Kaui	4683686.3	14722075	53831	22.0964	-159.5261
Starbuck	4683703.3	51673568	188592	-5.6384	-155.8811
Niihau	4683704.3	17098607	62505	21.85115	-160.18327
Molokai	4683712.3	31626104	115424	21.17481	-156.8214
Lisianski	4683718.3	51289619	187189	25.98702	-173.99438
Malden Atoll	4683720.3	68368950	249522	-4.0123	-154.9178
French Frigate Shoals	4683731.3	12353528	45131	23.87748	-166.29115
Hawaii	4683733.3	30728163	112147	20.00324	-155.83318
French Frigate Shoals	4683745.3	64763334	236363	23.6417	-155.8778
Lanaii	4683746.3	38160746	139273	20.76167	-156.8334
Millenium Atoll	4683747.3	71166319	259736	-9.9138	-150.2038
Pearl & Hermes Reef Wreck*	4574481.3	24339533	88980	27.8666	-175.7468
Caroline Wreck Site*	4574475.3	11555298	42262	-9.9957	-150.2161

936

Supplementary Table 2: Parameters and values used in the qualitative ecosystem model. To isolate the effect of bacterial and viral proliferative genes on algal, coral, bacteria, and viral populations, as many parameters as possible were held constant, and only those relating directly to bacterial and viral proliferation and pathogenicity changed (listed in **bold**). All populations, shown with arbitrary units to show relative change in Figure 5, were initialized at 0.5. Note that, to account for finite space on the benthos, algal population size A is solved from coral population size C as A = 1 – C each iteration. Code can be found at https://github.com/hopefulmonstersucla/viral-metabolism/tree/main/code.

Parameter	Symbol	Healthy reef without viruses	Degraded reef without viruses	Healthy reef with viruses	Degraded reef with viruses	Healthy reef with viruses and viral metabolism	Degraded reef with viruses and viral metabolism
Bacterial replication	m	0.02	0.2	0.02	0.2	0.02	0.2
Bacterial inhibition of coral	d	0.02	0.2	0.02	0.2	0.02	0.2
Coral replication	c	0.2	0.2	0.2	0.2	0.2	0.2
Algal inhibition of coral	i	0.02	0.02	0.02	0.02	0.02	0.02
Algal support of bacteria	a	0.2	0.2	0.2	0.2	0.2	0.2
Viral replication	l	-	-	-	-	0.2	0.02
Viral lysis of bacteria	k	-	-	0.2	0.02	0.2	0.02
Bacterial support of viral replication	k	-	-	0.2	0.02	0.2	0.02
Viral support of bacterial replication	t	-	-	-	-	0.02	0.2
Bacterial initial population	B	0.5	0.5	0.5	0.5	0.5	0.5
Coral initial population	C	0.5	0.5	0.5	0.5	0.5	0.5
Algal initial population	A	0.5	0.5	0.5	0.5	0.5	0.5
Viral initial population	V	-	-	0.5	0.5	0.5	0.5

948 **Supplementary Table 3: The frequency of photosynthesis genes across the lytic-**
949 **temperate spectrum.** Genes were identified using SEED Level 2 categorization
950 and are organized according to the KEGG photosynthesis map. Spearman's
951 Rho values indicate whether genes are over-represented (value < 0) or under-
952 represented (value > 0) in lytic versus temperate viral communities.

Level 2 Category	Photosystem	Function	Gene	Rho
Electron transport and photophosphorylation	Photosystem_II	photosystem II protein D1	PsbA	-0.845344
Electron transport and photophosphorylation	Photosystem_II	photosystem II protein D2	PsbD	-0.7327776
Electron transport and photophosphorylation	Photosystem_II	Cytochrome b559 beta chain	PsbF	-0.3442652
Electron transport and photophosphorylation	Photosystem_II	Photosystem II 10 kDa phosphoprotein	PsbH	0.04303315
Electron transport and photophosphorylation	Photosystem_II	Photosystem II protein	PsbN	-0.400914
Electron transport and photophosphorylation	Photosystem_II	Photosynthetic reaction center H subunit		-0.1290994
Electron transport and photophosphorylation	Photosystem_II	Putative photosynthetic complex assembly protein		0.2581989
Electron transport and photophosphorylation	Photosystem_I	photosystem I P700 chlorophyll a apoprotein subunit Ia	PsaA	-0.5610839
Electron transport and photophosphorylation	Photosystem_I	photosystem I P700 chlorophyll a apoprotein subunit Ib	PsaB	-0.6837071
Electron transport and photophosphorylation	Photosystem_I	photosystem I iron-sulfur center subunit VII	PsaC	-0.4461846
Electron transport and photophosphorylation	Photosystem_I	photosystem I subunit II	PsaD	-0.5711162
Electron transport and photophosphorylation	Photosystem_I	photosystem I subunit IV	PsaE	-0.502189
Electron transport and photophosphorylation	Photosystem_I	photosystem I subunit III plastocyanin docking protein	PsaF	-0.04303315
Electron transport and photophosphorylation	Photosystem_I	photosystem I subunit IX	PsaJ	-0.3442652
Electron transport and photophosphorylation	Photosystem_I	photosystem I subunit X	PsaK	-0.2484191
Light-harvesting complexes	Bacterial_light-harvesting_proteins	Light-harvesting LHI, beta subunit		0.1290994
Light-harvesting complexes	Chlorosome	Chlorosome protein I, 2Fe-2S ferredoxin		-0.2151657
Rhodopsins	Bacteriorhodopsin	Brp-like protein		-0.1844696
Rhodopsins	Proteorhodopsin	Octaprenyl-diphosphate synthase		0.1290994
Rhodopsins	Proteorhodopsin	Proteorhodopsin		-0.4655338

953

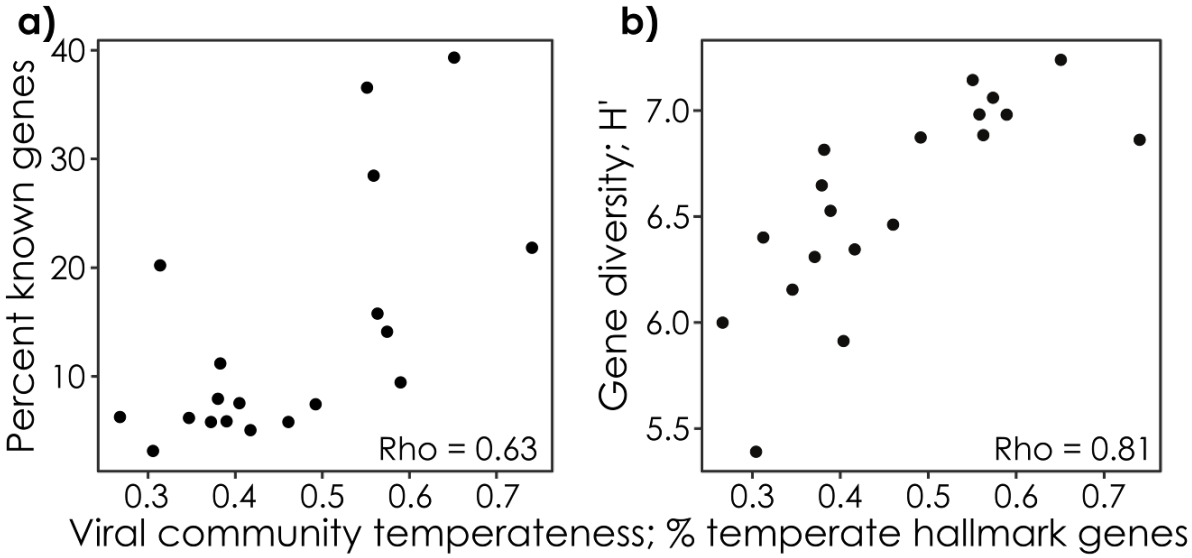

Supplementary Figure 1: Temperate viral communities are more cell-like and are more genetically diverse in known genes. (a) The percent of genes with hits against the SEED database (i.e., percent known genes), and (b) the diversity of those known genes in the viral communities across the lytic to temperate spectrum. Note that the percent known genes is indicative of how metabolically similar the viruses are to cells given that known genes are commonly of identified in the study of cells. Viral community temperateness was calculated as the percentage of integrase and excision genes in the known genes in each virome.

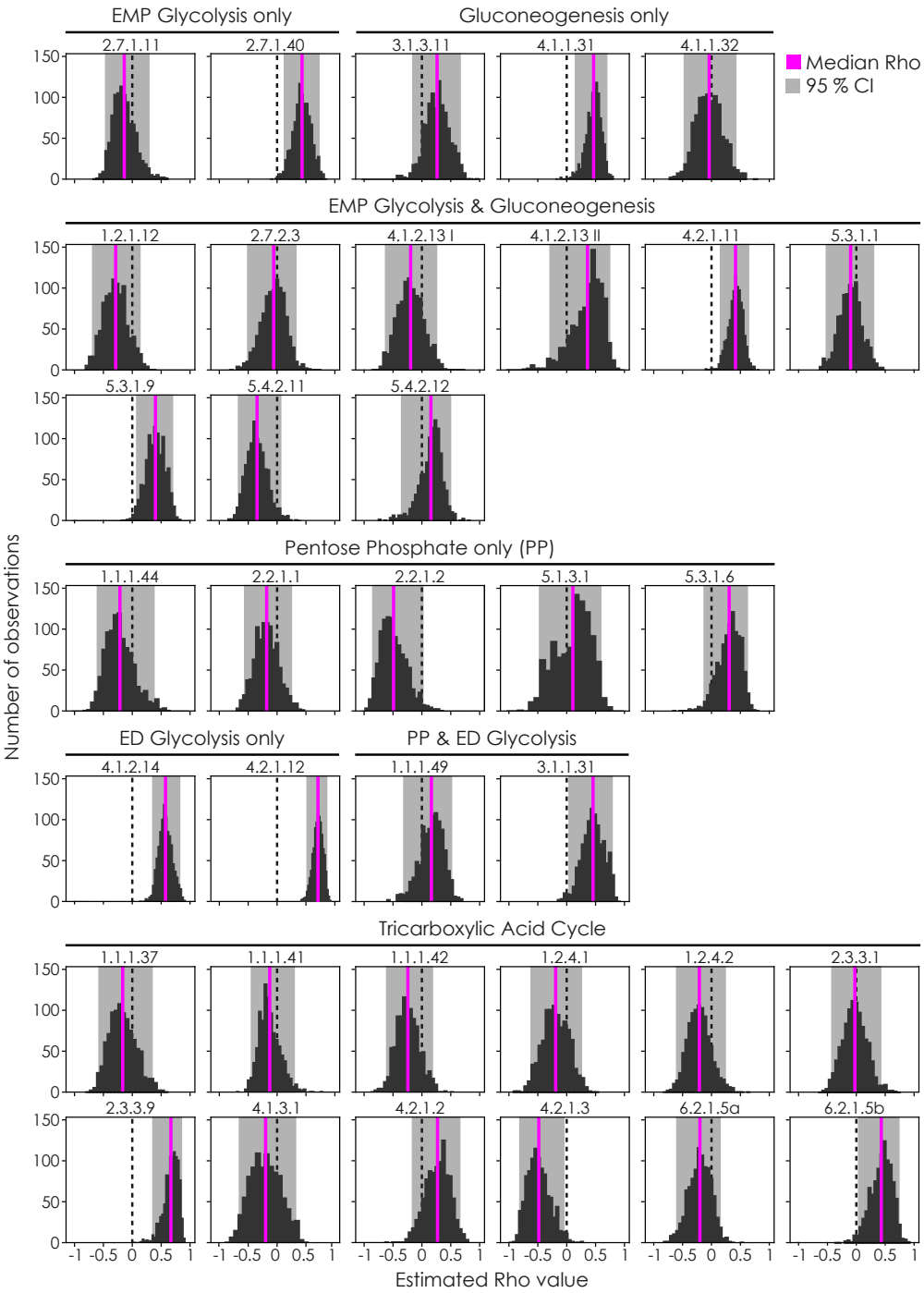

Supplementary Figure 2: Bootstrapped distribution of ρ_s from 1,000 iterations correlating the frequency of central carbon metabolism genes with viral community temperateness (number of observations vs ρ_s value). Genes are grouped by pathway. Histogram shows the distribution of bootstrapped ρ_s values, with pink lines showing the median bootstrapped value and shaded grey areas showing the 95 % confidence interval of the median ρ_s. Dashed vertical lines show $\rho_s = 0$. Bootstrapping code can be found at https://github.com/hopefulmonstersucla/viral-metabolism/tree/main/code.